

1 **Use of machine learning to estimate statistics of the**
2 **posterior distribution in probabilistic inverse problems**
3 **- an application to airborne EM data.**

4 **T. M. Hansen¹ and C. C. Finlay²**

5 ¹Department of Geoscience, Aarhus University, Denmark

6 ²DTU Space, Technical University of Denmark, Kgs. Lyngby, Denmark

7 **Key Points:**

- 8 • A machine learning approach for the probabilistic solution of inverse problems by
9 directly estimating posterior statistics of any continuous or discrete feature of the
10 posterior distribution.
11 • Allows the use of complex prior information and noise models.
12 • Demonstrated on nonlinear probabilistic inversion of airborne electromagnetic; en-
13 ables analysis of more than 100000 1D soundings per second.

Corresponding author: Thomas Mejer Hansen, tmeha@geo.au.dk

Abstract

The solution to a probabilistic inverse problem is the posterior probability distribution for which a full analytic expression is rarely possible. Sampling methods are therefore often used to generate a sample from the posterior. Decision-makers may be interested in the probability of features related to model parameters (for example existence of a pollution or the cumulative clay thickness) rather than the individual realizations themselves. Such features and their associated uncertainty, are simple to compute once a sample from the posterior distribution has been generated. However, sampling methods are often associated with high computational costs, especially when the prior and posterior distribution is non-trivial (non-Gaussian), and when the inverse problem is non-linear. Here we demonstrate how to use a neural network to directly estimate posterior statistics of any continuous or discrete feature of the posterior distribution. The method is illustrated on a probabilistic inversion of airborne EM data, where the forward problem is non-linear and the prior information is non-Gaussian. Once trained the application of the network is fast, with results similar to those obtained using much slower sampling methods.

1 Introduction

A key challenge in geoscience is that of combining different kinds of geo-information into one geo-model, typically describing the subsurface. This information can be direct information about geological processes, spatial variability, or it can be indirect information from measurements of properties related to the subsurface, such as geophysical data. Ideally, when such a geo-model has been established, one should be able to quantify information about specific features related to the geo-model, consistent with all information.

This integration of geo-information is typically solved using inverse problem theory (Tarantola & Valette, 1982a; Menke, 2012). Fast deterministic methods exist and have been widely used. For such methods, the goal is to obtain one optimal model, such as the simplest possible model, consistent with available information, typically in the form of observed data (Tikhonov, 1963; Menke, 2012; Constable et al., 1987). In practice, in part due to noise on data and model nonlinearities and imperfections, infinitely many models exist that will be consistent with data, and the deterministic approach can in general not account properly for such uncertainty.

Probabilistic inversion methods can, in principle, take into account arbitrarily complex information, and integrate the information into one consistent model, as given by the posterior probability distribution. A full analytic expression of the posterior distribution is rarely possible. Instead, sampling methods can be used to generate a sample of the posterior, which is a collection of realizations of the posterior distribution. From such a sample, the posterior statistics of any feature related to the model parameters can be computed. The probabilistic approach is therefore ideal for decision-makers for uncertainty quantification, as it allows probabilistic analysis and risk assessment consistent with available information.

The main obstacle to applying the probabilistic methodology in practice is that sampling methods are computationally very demanding (Hastings, 1970; Mosegaard & Tarantola, 1995). Sampling-based methods typically require both sampling or evaluation of a prior model, and evaluation of the physical forward response(s), many times.

One approach for reducing the computational requirements is to make use of fast approximate forward modeling. This can be related to using simplified 1D forward modeling as opposed to 3D forward models, or by using approximate physical models, which leads to modeling errors that should be accounted for (Hansen et al., 2014; Madsen & Hansen, 2018; Köpke et al., 2018).

64 Machine learning algorithms, which are fast to evaluate once trained, have also been
 65 used to approximate the forward modeling (Hansen & Cordua, 2017; Conway et al., 2019;
 66 Moghadas et al., 2020; Bording et al., 2021). Unsupervised machine learning methods,
 67 for example Generative adversarial neural networks (GANs), have been used more gen-
 68 erally as a means of representing features in a prior dataset; once trained, these provide
 69 an efficient means of rapidly generating many prior realizations (Mosser et al., 2017; Laloy
 70 et al., 2018; Mosser et al., 2020).

71 Attempts have also been made to use machine learning methods to learn a map-
 72 ping from data to model that can directly solve the inverse problem. R oth and Taran-
 73 tola (1994) were among the first to solve an inverse problem in this way using a multi-
 74 layer perceptron neural network, and demonstrated an application of inversion of reflec-
 75 tion seismic data to obtain single estimates of 1D velocity profiles. Recently, several au-
 76 thors have further explored this approach for directly solving a geophysical inverse prob-
 77 lem, making use of convolutional neural networks (Puzryev & Swidinsky, 2019; Moghadas,
 78 2020; Bai et al., 2020). A drawback of such methods is that, as in the deterministic so-
 79 lution of an inverse problem, they estimate only a single model, typically without account-
 80 ing for uncertainty on geophysical data, and do not quantify the uncertainty on the pre-
 81 dicted model parameters.

82 An important step towards finding probabilistic solutions to inverse problems us-
 83 ing neural networks was made by Devilee et al. (1999) who considered training data sets
 84 consisting of realizations from the prior distribution and the corresponding forward sim-
 85 ulated data with and without noise. They then used neural networks to learn a set of
 86 probabilistic estimators about each model parameter, including median and equidistant
 87 histogram estimators. Meier et al. (2007) extended this work and used mixture density
 88 network (MDN) to estimate the parameters of a Gaussian mixture model representing
 89 a parametric distribution approximating the 1D marginal posterior distribution, and ap-
 90 plied it to the problem of estimating global crustal thickness maps and comparing to re-
 91 sults obtained using a Monte Carlo based sampling method. Several other applications
 92 of MDN to approximate the posterior distribution, for different geophysical problems,
 93 have followed (Shahraeeni & Curtis, 2011; de Wit et al., 2013; Earp & Curtis, 2020; Earp
 94 et al., 2020).

95 Zhang and Curtis (2020a) argue that it may be problematic to apply such MDN’s
 96 for higher dimensional inverse problems, and suggest to use variational inference (Blei
 97 et al., 2017) to estimate the mean and standard deviation of the (non-Gaussian) poste-
 98 rior distribution in a seismic tomographic inverse problem. This method has been de-
 99 veloped further for variational full waveform inversion and tomographic inversion using
 100 normalizing flows (Zhang & Curtis, 2020b; Zhao et al., 2022). In all these cases a uni-
 101 form prior was assumed.

102 Attempts have also been made to use so-called invertible neural networks to simul-
 103 taneously estimate both the forward and inverse mapping between data and model pa-
 104 rameters (Ardizzone et al., 2018). This approach, which has recently been applied to ge-
 105 ophysical data by Zhang and Curtis (2021), allows the generation of multiple realizations
 106 of the posterior distribution, from which properties of the posterior distribution can be
 107 estimated, although constructing invertible neural networks involves more work than tra-
 108 ditional neural networks and involves compromises related to the flexibility of the net-
 109 work.

110 Here we present a method where the goal is not primarily to estimate the marginal
 111 1D posterior distribution (as in works based on Meier et al. (2007)). Instead, we pro-
 112 pose and demonstrate a machine learning-based method that provides direct estimates
 113 of any desired statistical property (continuous or discrete) of the posterior distribution,
 114 including any feature or property that can be computed from realizations of an, in prin-

115 ciple arbitrarily complex, prior model. This is done without generating realizations of
 116 the posterior distribution.

117 Following Devilee et al. (1999) and Meier et al. (2007) we construct a finite size train-
 118 ing data set, representing the information available in any probabilistic formulation of
 119 the inverse problem, namely prior information and information about the forward model
 120 and the noise.

121 This is then used to train a neural network whose output parameterizes any de-
 122 sired statistical property of the posterior distribution for which a log-likelihood can be
 123 computed. These properties can for example represent a Gaussian, generalized Gaussian,
 124 log-normal, or a mixture model distribution, representing continuous model parameters.
 125 The output can also refer to the posterior probability of defined classes of model features
 126 of discrete model parameters. The neural network is designed to ensure that the esti-
 127 mated statistical properties of the posterior are similar to the same statistics derived from
 128 a sample of the posterior. Given a suitable training set the method provides accurate
 129 information regarding the specific properties of the posterior distribution that are of sci-
 130 entific interest in a given problem at a fraction of the time used by traditional sampling-
 131 based approaches.

132 In the following the method is first presented for probabilistic inverse problems in
 133 general, which can be considered as a generalization of the ideas proposed by Devilee et
 134 al. (1999) and later derived work e.g. Meier et al. (2007); Earp et al. (2020). Then, we
 135 demonstrate the method, applying it to non-linear probabilistic inversion of airborne elec-
 136 tromagnetic data with non-Gaussian prior models of varying complexity. We show the
 137 neural network approach can be used to accurately estimate statistical properties of the
 138 posterior, related to both discrete and continuous model parameters, using regression
 139 and classification networks. The results are compared to results obtained by calculat-
 140 ing the same statistical properties from a sample of the posterior obtained using the ex-
 141 tended rejection sampler.

142 2 Method

143 Let $\mathbf{m} = [m_1, m_2, \dots, m_{N_M}]$ represent N_M model parameters that define some
 144 properties of a system, such as for example physical properties of a geo-model. \mathbf{m} is typ-
 145 ically represented on a grid in a Cartesian or spherical coordinate system. For example,
 146 \mathbf{m} might represent geophysical properties such as resistivity, velocity, or any other ge-
 147 ological/geophysical/geochemical parameter.

A key issue in geosciences is how to infer information about \mathbf{m} from different types
 of available information, such as geological expert knowledge, geophysical data, well log
 data, etc. This is generally referred to as an inverse problem. Tarantola and Valette (1982b)
 describe the inverse problem as a problem of probabilistic conjunction of information.
 Available information about \mathbf{m} is described in the form of probability densities and then
 combined using conjunction of information to obtain a single probability density that
 describes the combined information. For example, consider a case when a specific type
 of information about structural properties is quantified by $\rho(\mathbf{m})$, and that information
 from observed electromagnetic data and well logs is quantified through $L(\mathbf{m})$. Then the
 conjunction of this information is given by the posterior probability distribution $\sigma(\mathbf{m})$,
 which, under the assumption that the individual types of information have been obtained
 independently, is given by

$$\sigma(\mathbf{m}) \propto \rho(\mathbf{m}) \cdot L(\mathbf{m}). \quad (1)$$

In other words, the conjunction of the independent information is proportional to the
 product of probability densities describing each independent set of information. The like-
 lihood $L(\mathbf{m})$ is a measure of how well the data \mathbf{d} computed from a specific model matches

observed data \mathbf{d}_{obs} given noise with a specified probability distribution. Noise-free data can be computed by evaluating the forward model

$$\mathbf{d} = g(\mathbf{m}), \quad (2)$$

148 where g is a non-linear operator that maps the model parameters into data. g typically
149 refers to some numerical algorithm solving some physical equations (such as Maxwell's
150 equations).

151 The probabilistic inverse problem is then to infer information about $\sigma(\mathbf{m})$, which
152 contains the combined information of, for example, both structural prior information,
153 through the prior $\rho(\mathbf{m})$, and information from observed geophysical data, through $L(\mathbf{m})$.

154 A general approach (that allows using a non-linear forward model and non-Gaussian
155 prior) for solving probabilistic formulated inverse problems is use of sampling methods
156 to sample the posterior distribution, Eqn. 1, (Metropolis et al., 1953; Hastings, 1970; Ge-
157 man & Geman, 1984; Green, 1995; Mosegaard & Tarantola, 1995; Laloy & Vrugt, 2012;
158 Hansen et al., 2013, 2016). Unfortunately, such sampling methods can be extremely com-
159 putationally demanding, to the point where they cannot be practically applied. They
160 rely on solving the forward problem, Eqn. 2, many (often millions of) times.

161 Some algorithms make implicit assumptions about the prior model, such as a lay-
162 ered subsurface (Malinverno, 2002; Sambridge et al., 2013), while others, such as the clas-
163 sical rejection sampler and Metropolis algorithm (Hastings, 1970) require that both the
164 prior and likelihood can be evaluated. This typically leads to using relatively simple prior
165 models.

166 The extended variations of the Metropolis algorithm (Mosegaard & Tarantola, 1995)
167 and the rejection sampler (Hansen et al., 2016; Hansen, 2021) do not require that an an-
168 alytical description of the prior exists, as evaluation of the prior is not needed. It is suf-
169 ficient that an algorithm exists that can generate a realization from the prior. This opens
170 up the possibility of using a variety of more complex prior models, based on for exam-
171 ple geostatistical simulation-based methods (Hansen et al., 2008, 2012).

172 2.1 Properties related to geophysical model parameters.

173 The model parameters \mathbf{m} typically refer to physical parameters (e.g. resistivity when
174 dealing with electromagnetic (EM) data, or elastic properties when dealing with seismic
175 data). In practice, decision makers may be more interested in related features, or spe-
176 cific questions, such as "What is the chance of penetrating a specific lithology when drilling?"
177 (Scales & Snieder, 1997). Such features or occurrences of events will be referred to through
178 \mathbf{n} .

In general the relation between \mathbf{m} and \mathbf{n} can be complex and is formally described
by a joint prior distribution $\rho(\mathbf{m}, \mathbf{n})$. This can for example be the case if \mathbf{n} refers to sub-
surface lithology, and \mathbf{m} to a geophysical property. This has been widely studied in the
inversion of reflection seismic data, where information about geophysical properties is
often assumed dependent on lithology, such that $\rho(\mathbf{m}, \mathbf{n}) = \rho(\mathbf{n})\rho(\mathbf{m}|\mathbf{n})$ (Bosch et al.,
2010; Grana & Della Rossa, 2010; Rimstad et al., 2012). A more general formulation of
Eqn. 1, describing information on both \mathbf{m} and \mathbf{n} is then

$$\sigma(\mathbf{m}, \mathbf{n}) \propto \rho(\mathbf{m}, \mathbf{n}) \cdot L(\mathbf{m}, \mathbf{n}), \quad (3)$$

given the available joint prior information, the forward model, and the noise. The cor-
responding forward problem, generalizing Eqn. 2, takes the form

$$\mathbf{d} = g(\mathbf{m}, \mathbf{n}). \quad (4)$$

179 Sometimes the relation between \mathbf{m} and \mathbf{n} is so simple that \mathbf{n} can be computed from
180 \mathbf{m} through a mapping function $\mathbf{n} = h(\mathbf{m})$. For example, \mathbf{n} can refer to the volume of

181 a reservoir (a scalar) obtained from a high dimensional set of geophysical model param-
 182 eters \mathbf{m} . Or, \mathbf{n} can refer to the cumulative thickness of layers with a resistivity (\mathbf{m}) above
 183 some threshold. Another example is when \mathbf{m} refers to properties of a groundwater model.
 184 Then flow modeling based on a set of realizations from the posterior, can be used to prop-
 185 agate uncertainties into for example, the arrival time of polluted groundwater (\mathbf{n}) at a
 186 specific location (Vilhelmsen et al., 2019). Such a focus on related features and proper-
 187 ties derived from the posterior distribution, rather than the posterior distribution over
 188 the geophysical parameter $\sigma(\mathbf{m})$ itself, is discussed by Scheidt et al. (2015).

189 The sampling algorithms described above can be used to generate a sample from
 190 $\sigma(\mathbf{m}, \mathbf{n})$ from which statistical analysis of any feature related to $\sigma(\mathbf{m}, \mathbf{n})$ can be computed.
 191 This is computationally demanding, and in many cases decision-makers are more inter-
 192 ested in the statistical analysis of features and properties of the posterior distribution
 193 rather than the actual realizations.

194 Here a method is proposed that allows direct computation of properties and fea-
 195 tures of $\sigma(\mathbf{m}, \mathbf{n})$, using a neural network trained on a data set representing a sample of
 196 known information (including the prior, forward, noise and modeling errors), without
 197 ever generating realizations of $\sigma(\mathbf{m}, \mathbf{n})$. The approach follows the basic strategy suggested
 198 by Devilee et al. (1999), and consists of two steps: A) construction of a training data set,
 199 and B) construction and training of a neural network. This is done once. Then, the trained
 200 machine learning algorithm can be applied, very efficiently to compute desired properties
 201 of the posterior distribution, for potentially many sets of observed data.

202 2.2 A: Construction of training data set

Eqn. 4 describes the forward problem of computing noise free data. The forward
 problem describing simulation of data including noise, \mathbf{d}_{sim} is

$$\mathbf{d}_{sim} = g(\mathbf{m}, \mathbf{n}) + r(\mathbf{m}, \mathbf{n}) = \mathbf{d} + r(\mathbf{m}, \mathbf{n}), \quad (5)$$

203 where $r(\mathbf{m}, \mathbf{n})$ is a realization of an assumed noise model. Often geophysical data \mathbf{d} de-
 204 pends only directly on the physical parameters, in which case $g(\mathbf{m}, \mathbf{n}) = g(\mathbf{m})$.

Let $\mathbf{M}^* = [\mathbf{m}^{1*}, \mathbf{m}^{2*}, \dots, \mathbf{m}^{N_T^*}]$ and $\mathbf{N}^* = [\mathbf{n}^{1*}, \mathbf{n}^{2*}, \dots, \mathbf{n}^{N_T^*}]$ represent N_T re-
 alizations of $\rho(\mathbf{m}, \mathbf{n})$. Let $\mathbf{D}^* = [\mathbf{d}^{1*}, \mathbf{d}^{2*}, \dots, \mathbf{d}^{N_T^*}]$ represent the corresponding N_T noise
 free data, obtained by evaluating Eqn. 4. Finally let $\mathbf{D}_{sim}^* = [\mathbf{d}_{sim}^{1*}, \mathbf{d}_{sim}^{2*}, \dots, \mathbf{d}_{sim}^{N_T^*}]$ rep-
 resent N_T corresponding realizations of simulated noisy data, following Eqn. 5. This con-
 stitutes a training data set

$$\mathbf{T} = [\mathbf{N}^*; \mathbf{M}^*; \mathbf{D}^*; \mathbf{D}_{sim}^*], \quad (6)$$

205 that can be obtained by 1) sampling the prior, 2) solving the forward problem, 3) sim-
 206 ulation of the noise.

207 The sample \mathbf{T} in Eqn. 6 represents the available information (prior, physics of the
 208 forward model, noise) in so far as it can be represented by a finite sample of size N_T . The
 209 larger the sample, the more complete the representation of the available information.

210 2.2.1 Infinite training data

211 Consider first the hypothetical limiting case when \mathbf{T} is infinitely large ($N_T \rightarrow \infty$).
 212 In this case, \mathbf{T} represents not just a subset of the available information, but all available
 213 information. The full probability distribution over any sets of parameters \mathbf{n} , \mathbf{m} , \mathbf{d} , and
 214 \mathbf{d}_{sim} can be fully reconstructed from \mathbf{T} . Say some data have been measured as \mathbf{d}_{obs} . The
 215 corresponding inverse problem can then be solved simply by locating all the sets of mod-
 216 els $[\hat{\mathbf{m}}, \hat{\mathbf{n}}] = ([\hat{\mathbf{m}}^{1*}, \hat{\mathbf{m}}^{2*}, \dots], [\hat{\mathbf{n}}^{1*}, \hat{\mathbf{n}}^{2*}, \dots])$ in \mathbf{T} for which $\mathbf{d}_{sim}^{i*} = \mathbf{d}_{obs}$. $[\hat{\mathbf{m}}, \hat{\mathbf{n}}]$ will then
 217 represent a sample of $\sigma(\mathbf{m}, \mathbf{n})$ consisting of all possible realizations.

218 The goal here is not to generate realizations of the posterior, but instead to com-
 219 pute statistical properties of the posterior. In other words, given a sample $\hat{\mathbf{n}}$ of the pos-
 220 terior, $\sigma(\mathbf{n})$, the goal is to compute parameters Θ that define a desired statistical prop-
 221 erty of $\sigma(\mathbf{n})$. For example, if \mathbf{n} refers to a discrete parameter with N_o possible outcomes,
 222 then $\Theta = [\theta_1, \dots, \theta_{N_o}]$ could refer to the probability of realizing each possible outcome.
 223 If \mathbf{n} refers to a continuous parameter, $\Theta = [\theta_0, \mathbf{C}_\theta]$ could represent the mean and co-
 224 variance of a multivariate Gaussian distribution. $\Theta = [\theta_0, \theta_1, \theta_2]$ could represent the
 225 mean, variance and power of a generalized 1D Gaussian distribution. $\Theta = [\theta_0]$ could
 226 represent the rate of a Poisson distribution. $\Theta = [\theta_0, \theta_1]$ could represent a Binomial dis-
 227 tribution.

The optimal values of Θ , given a sample $\hat{\mathbf{n}}$ of $\sigma(\mathbf{n})$, can be found maximizing the likelihood, L_Θ that each realization of the posterior is a realization of the probability distribution (defined by the parameter Θ)

$$L_\Theta = f(\hat{\mathbf{n}}|\Theta) = \prod_{i=1}^{N_\sigma} f(\hat{\mathbf{n}}^{i*}|\Theta), \quad (7)$$

where N_σ is the number of realizations of $\hat{\mathbf{n}}$. Maximization of Eqn. 7 is equivalent to minimizing the negative log-likelihood (which we refer to as the loss J_Θ):

$$J_\Theta = -\log\left(\prod_{i=1}^{N_\sigma} f(\hat{\mathbf{n}}^{i*}|\Theta)\right) \quad (8)$$

$$= -\sum_{i=1}^{N_\sigma} \log(f(\hat{\mathbf{n}}^{i*}|\Theta)). \quad (9)$$

228 Minimization of the loss function, Eqn. 9, can be used to obtain estimates of Θ repre-
 229 senting a desired statistical property of $\sigma(\mathbf{n})$.

2.2.2 Finite training data

230 Use of an infinite training dataset is obviously unrealistic. Instead, we use a finite-
 231 sized training data \mathbf{T} to design and train a neural network to estimate Θ directly from
 232 realizations of simulated data including noise \mathbf{d}_{sim}^{i*} . It is trained by maximization of the
 233 probability that \mathbf{n}^{i*} are realizations of the chosen probability distribution, described by
 234 Θ , which are the result of evaluating the neural network $\mathbf{d}_{sim}^{i*} \mapsto \Theta$.
 235

236 To achieve this, we make use of the fact that a particular feature or derived prop-
 237 erty in the training data set, \mathbf{n}^{i*} , is a realization of the posterior distribution $\sigma(\mathbf{n})$ one
 238 would get from probabilistic inversion of \mathbf{d}_{sim}^{i*} , as discussed above in 2.2.1.

239 If enough training data are available and a neural network complex enough to en-
 240 compass the available information can be trained, then the network will estimate the sta-
 241 tistical parameters Θ characterizing the desired properties of the posterior distribution
 242 $\sigma(\mathbf{m}, \mathbf{n})$.

2.3 B: Construct and train a neural network to estimate relevant statistics of $\sigma(\mathbf{m}, \mathbf{n})$

243 In principle any machine learning method capable of regression and/or classifica-
 244 tion, such as regression trees and support vector machines (Bishop et al., 1995), can be
 245 used to estimate the mapping $\mathbf{d}_{sim}^* \mapsto \Theta$ which after training can be used to evaluate
 246 $\mathbf{d}_{obs} \mapsto \Theta$. Here we use make use of a fully connected artificial neural network. The pre-
 247 sented approach builds on earlier work by Röth and Tarantola (1994), Devilee et al. (1999)
 248 and Meier et al. (2007).
 249
 250

A neural network is arranged into a number of layers, each consisting of a number of neurons. Each neuron has two adjustable parameters, the weight w , and the bias b , as well as an activation function Ψ . All neurons in one layer are fully connected to all neurons in the following layer. The input for a neuron (except for the first layer where the input is \mathbf{d}_{sim}^*) is the output of the neurons in the previous layer, and the output y_j of a neuron in response to inputs x_i , is given by

$$y_j = \Psi \left(\sum_i (w_i * x_i) + b \right)$$

251 For a specific network, with specified values for the weights and biases, one can compute
 252 the output, given some input, simply by evaluating the neurons layer by layer, starting
 253 from the input layer. See e.g. Bishop et al. (1995) for more details. To learn a partic-
 254 ular mapping, the parameters of the neural network are adjusted to minimize a loss func-
 255 tion that quantifies the performance of the network based on the training dataset. The
 256 choice of loss function is key to how the output of the neural network can be interpreted.

257 **2.3.1 The structure of the neural network**

258 A neural network can be described in terms of an input layer, the central inner part
 259 of the neural network (which can consist of many layers, referred to as hidden layers),
 260 and an output layer.

261 The input layer here represents the training data, which include noise, and consists
 262 of N_d nodes. The output layer has N_θ nodes representing the statistical parameters de-
 263 scribing a distribution characterizing the features or properties of the posterior distri-
 264 bution that one wishes to predict.

265 The inner part of the network can be either simple or complex, and it can consist
 266 of either (fully) connected layers, convolutional layers, or combinations of these and other
 267 types of layers depending on the application. Here a fully connected neural network is
 268 considered as it has been demonstrated that such a neural network, with at least one hid-
 269 den layer, can approximate any continuous function with arbitrary accuracy, when the
 270 number of hidden units is large enough (Hornik et al., 1990).

271 **2.3.2 The loss function**

272 When a neural network is trained using the training data set, its free parameters
 273 (the weight and bias of each node for a fully connected network) are adjusted to min-
 274 imize a specific loss function. In the present case, the training data set consists of (when
 275 properties of $\sigma(\mathbf{n})$ are of interest) $\mathbf{T} = [\mathbf{N}^*; \mathbf{D}_{sim}^*]$. The goal is to estimate $\mathbf{d}_{sim}^* \mapsto \Theta$
 276 rather than simply $\mathbf{d}_{sim}^* \mapsto \mathbf{n}$.

277 This is achieved by constructing a loss function where the unknown parameters Θ
 278 describe statistical properties of the desired probability distribution, Eqn. 7, whose pa-
 279 rameters can be found by minimizing the loss function, Eqn. 9. The key here is to use
 280 a loss function that represents the negative log-likelihood of the probability distribution
 281 whose parameters Θ one wishes to estimate.

282 At each iteration of training the neural network, the loss is computed by applying
 283 the following steps for each dataset $T^i = [\mathbf{n}^{i*}, \mathbf{d}_{sim}^{i*}]$ in the training data set \mathbf{T} :

- 284 1. Evaluate the network using \mathbf{d}_{sim}^{i*} as input. This provides as output an estimate
 285 $\hat{\Theta}_i$
- 286 2. Evaluate the corresponding loss, J^i , as $J^i = -\log(f(\mathbf{n}^{i*}|\hat{\Theta}_i))$.

The total loss is then given by

$$\mathbf{J} = \sum_{i=1}^{N_T} J^i. \quad (10)$$

287 \mathbf{n}^{i*} is a realization of $\sigma(\mathbf{n})$, given the data \mathbf{d}_{sim}^{i*} , and therefore, minimizing the loss in
 288 Eqn. 10 leads to estimates of statistical parameters Θ that describe $\sigma(\mathbf{n})$, in the same
 289 manner as would minimizing Eqn. 9 given a sample, $\hat{\mathbf{n}}$, of $\sigma(\mathbf{n})$. The difference is that
 290 the proposed method achieves this without the need to first realize the sample $\hat{\mathbf{n}}$ of $\sigma(\mathbf{n})$.

291 Minimizing the loss function thus maximizes the probability that each \mathbf{n}^{i*} can be
 292 seen as a realization of the probability distribution whose parameters Θ_i are the result
 293 of evaluating the neural network $\mathbf{d}_{sim}^{i*} \mapsto \Theta_i$.

294 In general, \mathbf{n} (and/or \mathbf{m}) can refer to a continuous parameter (such as velocity,
 295 resistivity, temperature, or related properties) or a discrete parameter (such as lithol-
 296 ogy type and event type). Continuous model parameters typically lead to a regression
 297 type problem, whereas discrete model parameters lead to a classification problem.

298 *2.3.2.1 Continuous model parameters - regression* Here we first consider the case
 299 when \mathbf{n} represents continuous parameters. Say we wish to estimate the mean and co-
 300 variance, $\hat{\Theta}_0$ and $\hat{\mathbf{C}}_\theta$, of the posterior distribution $\sigma(\mathbf{n})$ given a set of observed data \mathbf{d}_{obs} .

Assume a neural network exists that outputs a set of parameters describing $\Theta =$
 $[\hat{\Theta}_0^i, \hat{\mathbf{C}}_\theta^i]$, given the input \mathbf{d}_{sim}^i . The likelihood that a set of parameters from the train-
 ing dataset \mathbf{n}^{i*} is a realization from the multivariate Gaussian distribution $\mathcal{N}(\hat{\Theta}_0^i, \hat{\mathbf{C}}_\theta^i)$
 as obtained from evaluating the neural network using \mathbf{d}_{sim}^{i*} as input, is given by

$$f(\mathbf{n}^{i*} | \hat{\Theta}_0^i, \hat{\mathbf{C}}_\theta^i) = k_C \exp(-0.5 (\mathbf{n}^{i*} - \hat{\Theta}_0^i)^T \hat{\mathbf{C}}_\theta^{i-1} (\mathbf{n}^{i*} - \hat{\Theta}_0^i)), \quad (11)$$

where $k_C = ((2\pi)^{N_d} |\hat{\mathbf{C}}_\theta^i|)^{-0.5}$ is a normalization factor. The corresponding loss function
 J^i is the negative log-likelihood loss function, that is

$$J^i = -\log(f(\mathbf{n}^{i*} | \hat{\Theta}_0^i, \hat{\mathbf{C}}_\theta^i)) \quad (12)$$

$$= -0.5 (\mathbf{n}^{i*} - \hat{\Theta}_0^i)^T \hat{\mathbf{C}}_\theta^{i-1} (\mathbf{n}^{i*} - \hat{\Theta}_0^i) \quad (13)$$

301 The total average loss is then given by Eqn. 10.

302 Any machine learning method that minimizes this loss function, will lead to a neu-
 303 ral network that provides an estimate of the parameters of interest, here $\Theta = [\hat{\Theta}_0, \hat{\mathbf{C}}_\theta]$,
 304 that are computed directly without ever computing realizations of $\sigma(\mathbf{n})$.

305 To represent the posterior mean and full covariance, given N_m model parameters,
 306 an output layer of $N_\Theta = N_m + N_m^2$ nodes must be used. If only the posterior mean
 307 and variance are estimated, an output layer of $N_\Theta = N_m + N_m$ nodes is needed. If only
 308 the posterior mean is of interest an output layer of $N_\Theta = N_m$ nodes is needed and min-
 309 imizing Eqn. 13 is then similar to minimizing the widely used mean squared error loss
 310 function (Bishop et al., 1995), as utilized for example in e.g. Röth and Tarantola (1994).

311 Recall, that the above scheme does not impose any assumptions on either the prior
 312 or the posterior distribution which may be complex. The estimated mean and covari-
 313 ance are simply statistical parameters of the posterior distribution, that may or may not
 314 be useful for a specific use case.

315 The quality of the obtained estimate naturally depends on the complexity of the
 316 machine learning model used, and the size of the training data set, which will be con-
 317 sidered in more detail in the application presented below.

318 Other statistical parameters of the posterior can be estimated by minimizing the
 319 appropriate log-likelihood function for the corresponding probability distribution.

For example, a 1D generalized probability distribution is defined by three parameters $\Theta = [\theta_1, \theta_2, \theta_3]$, and its probability distribution given by (Tarantola, 2005)

$$f(n^i|\Theta) = \frac{1}{2\theta_2\Gamma(1+1/\theta_3)} \exp\left(-\left(\frac{|n^i - \theta_1|}{\theta_2}\right)^{\theta_3}\right) \quad (14)$$

A 1D Gaussian mixture model based on a mixture of Nc 1D Gaussian distribution, as considered by e.g. Meier et al. (2007), is defined by $\Theta = [\mathbf{t}_1, \mathbf{t}_2, \mathbf{t}_3] = [t_1^1, \dots, t_1^{Nc}, t_2^1, \dots, t_2^{Nc}, t_3^1, \dots, t_3^{Nc}]$, where \mathbf{t}_1 refer to the mean, \mathbf{t}_2 refer to the standard deviation of Nc Gaussian distribution, each with weight \mathbf{t}_3 , and its probability distribution given by

$$f(n^i|\mathbf{t}_1, \mathbf{t}_2, \mathbf{t}_3) = \sum_{i=1}^{Nc} t_3^i (t_2^i \sqrt{2\pi})^{-1} \exp\left(-0.5\left(\frac{n^i - t_1^i}{t_2^i}\right)^2\right) \quad (15)$$

320 The corresponding log-likelihood of Eqn. 14 and 15 can trivially be obtained and used
 321 as a loss function in a neural network to estimate Θ . In principle, any statistical param-
 322 eters, for which the associated log-likelihood can be computed, and used as a loss func-
 323 tion, can be estimated using the proposed methodology.

324 *2.3.2.2 Discrete model parameters - classification* Say n_i represents a discrete
 325 parameter with N_o possible outcomes (classes). One's aim is then to estimate the pos-
 326 terior probability of each of the N_o classes given some data \mathbf{d}_{obs} .

327 Let $\theta_i^* = [p_i^{1*}, p_i^{2*}, \dots, p_i^{N_o*}]$ represent the true probabilities of n_i^* belonging to
 328 a specific class. In practice the true probability of one (the correct) class will be one, and
 329 the others zero. Further $\hat{\theta}_i = [\hat{p}_i^1, \hat{p}_i^2, \dots, \hat{p}_i^{N_o}]$ represent the corresponding predictions
 330 by the neural network of the probabilities of each class for a specific model parameter,
 331 n_i .

The likelihood of observing θ_i given $\hat{\theta}_i$ is then

$$f(\theta_i|\hat{\theta}_i) = \prod_{j=1}^{N_o} (\hat{p}_i^j)^{p_i^{j*}}. \quad (16)$$

The corresponding loss function J^i is then

$$J^i = -\log(f(\theta_i|\hat{\theta}_i)) = -\sum_{j=1}^{N_o} p_i^{j*} \log(\hat{p}_i^j). \quad (17)$$

332 The choice of class probabilities $\hat{\theta}_i$ that maximizes Eqn. 16 can be found by min-
 333 imizing the negative log-likelihood given by the loss function, Eqn. 17, which is equiv-
 334 alent to the categorical cross-entropy between the two probability distributions (Bishop
 335 et al., 1995). Usually, the softmax activation is used for multi-class classification prob-
 336 lems (and the sigmoid activation function for binary classification problems), as it forces
 337 all probabilities to be in the range 0 to 1, and ensures that $\sum_{j=1}^{N_o} \hat{p}_i^j = 1$, such that the
 338 output parameters can be interpreted as a probability. A neural network that estimates
 339 the mapping $\mathbf{d}_{sim}^i \mapsto \hat{\theta}_i$ by minimizing Eqn. 17, using the softmax activation function
 340 in the output layer, therefore locates the maximum-likelihood of Eqn. 16, which directly
 341 estimates $\sigma(p_i^*)$.

342 In other words, this method can be used to compute the posterior class probabil-
 343 ity of a discrete model parameter, without generating a sample of the posterior distri-
 344 bution.

345 To summarize, our proposed method involved first constructing a training data set
 346 (Eqn. 6) that represents (limited by the size of the used training data set) the known
 347 information (the prior, the forward, and the noise model), and specifically contains prior
 348 knowledge regarding any feature \mathbf{n} , that may be directly or indirectly related to the model
 349 parameters \mathbf{m} , about which one wishes to infer information. A neural network is then
 350 designed and trained by minimizing a specific loss function (that expresses the log-likelihood
 351 of the parameters Θ describing the probability distribution of desired features \mathbf{n} that may
 352 be either continuous or discrete.

353 **3 Results / Application to airborne EM data**

354 The methodology described above is applied to the inversion of airborne electro-
 355 magnetic (AEM) data. This inverse problem has been widely studied by deterministic
 356 linearized least-squares methods using both a 1D and 3D forward model (Christensen,
 357 2002; Auken & Christiansen, 2004; Viezzoli et al., 2008; Cox et al., 2010; Grayver et al.,
 358 2013; Auken et al., 2014).

359 The full non-linear 1D inverse problem has also been addressed using Markov chain
 360 Monte Carlo (MCMC) sampling methods, based on for example the reversible-jump sam-
 361 pling method relying on a prior model representing a 1D layered subsurface (B. J. Mins-
 362 ley, 2011; B. J. Minsley, Foks, & Bedrosian, 2021; Brodie & Sambridge, 2012). Hansen
 363 and Minsley (2019) proposed the use of extended Metropolis algorithm, also an MCMC
 364 method, that allows the use of any prior model that can be sampled. The 1D nonlinear
 365 inverse EM problem leads to a non-trivial sampling problem, due to the existence of model
 366 equivalences (significantly different models lead to the same forward response). Sufficient
 367 sampling of the 1D posterior distribution of resistivity values, to obtain a limited set of
 368 independent realizations, may require hundreds of thousands of MCMC iterations, and
 369 hence forward model evaluations. For a single sounding this may take at least 10 min-
 370 utes per sounding, requiring access to supercomputers for application of real-world data
 371 sets (Foks & Minsley, 2020). Hansen (2021) proposed 1D probabilistic inversion based
 372 on the extended rejection sampler (using lookup tables, similar to $[\mathbf{N}^*, \mathbf{M}^*, \mathbf{D}^*]$) that rely
 373 on the construction of a large sample for the prior along with the forward responses (gen-
 374 erated once). This is then used to generate independent realizations of the posterior dis-
 375 tribution numerically more efficiently than is possible using Markov Chain based algo-
 376 rithms, and at the same time avoids issues related to model equivalences. This sampling
 377 approach is used for comparison below.

378 The size of airborne EM surveys is becoming larger, so the use of any of the inver-
 379 sion methods discussed above will lead to considerable computational demands. Cur-
 380 rently, two major airborne EM surveys are being carried out. The AusAEM20 project,
 381 by Geoscience Australia, is expected to collect around 65000 flight-line-kilometer of data,
 382 leading to many hundreds of thousands of EM measurements (Howard, 2020). USGS has
 383 collected more than 43000 flight-line-kilometer data in the Mississippi Alluvial Plain, and
 384 another 25000 flight-line-kilometer is planned for 2021, leading to significantly more than
 385 1.000.000 data points to be inverted in the Mississippi Alluvial Plain (B. J. Minsley, Rigby,
 386 et al., 2021).

387 **3.1 AEM data from Morrill, Nebraska**

388 As an example we consider the inversion of airborne electromagnetic (AEM) data
 389 from Morrill, Nebraska (Smith et al., 2010; Abraham et al., 2012). The same profile of
 390 data obtained at 451 locations along a West-East profile is used here as described in B. J. Mins-
 391 ley (2011). Each observed data set consists of 12 measurements (in-phase and quadra-
 392 ture measurements from 6 pairs of transmitter and receiver coils).

Three different types of prior models will be defined, that represent different information about the subsurface resistivities (\mathbf{m}) and related (both discrete and continuous) properties \mathbf{n} at Morrill. For each of the three prior models considered, a unique posterior probability distribution exists. Various properties of the posterior distribution will be computed using the proposed machine learning method and compared to results obtained from a finite sample of the posterior distributions obtained using the extended rejection sampler with a lookup table of size $N_T = 2 \cdot 10^6$.

3.2 A priori models and noise

3.2.1 Parameterization

In this example, the subsurface is parameterized into 125 layers of $dz = 1$ m thickness. Prior models based on up to four sets of parameters, $\rho(\mathbf{m}, \mathbf{n}_1, \mathbf{n}_2, \mathbf{n}_3)$ are considered.

Resistivity. $\mathbf{m} = [m_1, m_2, \dots, m_{N_M}]$ represents the resistivity of each of the 125 layers.

Layer interface. \mathbf{n}_1 represents the existence of a sharp boundary between two neighboring layers ($n_{1i} = 0$ when there is no boundary and $n_{1i} = 1$ in case of a boundary). A sharp boundary is defined when two neighboring resistivity values differ more than 20%. \mathbf{n}_1 refers to 125 discrete parameters and can be directly computed from \mathbf{m} .

Thickness of highly resistive layer. \mathbf{n}_2 represent the cumulative thickness of resistivity values above 225 ohmm. \mathbf{n}_2 , which can be directly computed from \mathbf{m} using

$$\mathbf{n}_2 = \sum_i^{N_M} dz * I(m_i),$$

where $I(m_i) = 1$ when $m_i > 225$ ohmm, and $I(m_i) = 0$ when $m_i \leq 225$ ohmm. \mathbf{n}_2 refers to a single continuous parameter.

Lithology. \mathbf{n}_3 represents a category ('1', '2', and '3', representing three distinct lithologies) in each layer. \mathbf{n}_3 cannot be computed from \mathbf{m} , but \mathbf{n}_3 and \mathbf{m} are linked through a conditional prior distribution $\rho(\mathbf{m}|\mathbf{n}_3)$ (see example below). \mathbf{n}_3 refers to 125 discrete parameters with 3 possible outcomes.

For brevity, all model parameters combined will be referred to as $\mathbf{p} = [\mathbf{m}, \mathbf{n}_1, \mathbf{n}_2, \mathbf{n}_3]$. To illustrate the potential of the method 3 different non-Gaussian prior models are considered that vary in complexity and information content.

3.2.2 Prior information

$\rho_A(\mathbf{p}) = \rho_A(\mathbf{m}, \mathbf{n}_1, \mathbf{n}_2)$, a uniform prior model. $\rho_A(\mathbf{p})$ represents a choice of independence between model parameters, $\rho_A(m_i, m_j) = \rho_A(m_i)\rho_A(m_j) \forall (i, j)$. The resistivity of each resistivity model parameter is assumed to be log-uniform distributed in the range $\mathcal{U}[2, 2800]$ ohmm. This is the least informative prior model considered. 11 independent realizations of $\rho_A(\mathbf{m}, \mathbf{n}_1)$ are shown in Figure 1a.

$\rho_B(\mathbf{p}) = \rho_B(\mathbf{m}, \mathbf{n}_1, \mathbf{n}_2)$, Discrete layered model. $\rho_B(\mathbf{p})$ represents a layered subsurface consisting of 1 to 8 layers (uniformly distributed), each with a constant resistivity. The resistivity in a specific layer is assumed to be log-uniform distributed in the range $\mathcal{U}_{\uparrow}[2, 2800]$ ohmm.

A realization \mathbf{p}^* of $\rho_B(\mathbf{p})$ is generated by first choosing the number of layers as a random number, Nl , between 1 and 8. Then $Nl - 1$ layer interfaces are randomly selected from a uniform distribution of $\mathcal{U}[0, 125]$ m. Then the resistivity within each layer

433 is realized from a uniform distribution $\mathcal{U}_{\downarrow}[2, 2800]$ ohmm. This type of prior model is sim-
 434 ilar to the transdimensional prior considered by (B. J. Minsley, 2011). 11 independent
 435 realizations of $\rho_B(\mathbf{m}, \mathbf{n}_1)$ are shown in Figure 1b.

436 $\rho_C(\mathbf{p})$, *Trimodal mixture Gaussian*. $\rho_C(\mathbf{p})$ represents a subsurface with three pos-
 437 sible lithologies ('1', '2' and '3') each with a distinct resistivity distribution. See discus-
 438 sion about the prior geological knowledge in Morrill in Abraham et al. (2012) and Hansen
 439 and Minsley (2019).

440 To sample $\rho_C(\mathbf{p}) = \rho_A(\mathbf{m}, \mathbf{n}_1, \mathbf{n}_2, \mathbf{n}_3)$, first a realization of $\rho_C(\mathbf{n}_3)$ is generated
 441 as $\rho_C(\mathbf{n}_3^*)$, which represents an example of the distribution of the lithologies. This is
 442 achieved by generating a realization of a multivariate normal distribution with a Gaus-
 443 sian type covariance model with a range of 30 m, followed by a simple truncation to ob-
 444 tain 40% of lithology A, 40% of lithology B, and 20% of lithology C. Then a realization
 445 of the resistivity \mathbf{m}^* is generated, conditional to the lithology type from $\rho_C(\mathbf{m}|\mathbf{n}_3^*)$. The
 446 resistivity, within each lithology, is generated as a realization of a multivariate normal
 447 distribution in \log_{10} -resistivity space with a range of 30 m, a specific mean, m_0 and stan-
 448 dard deviation, m_{std} . For lithology '1', $m_0 = 1.1$ and $m_{std} = 0.14$. For lithology '2',
 449 $m_0 = 2$ and $m_{std} = 0.2$. For lithology '3', $m_0 = 2.75$ and $m_{std} = 0.25$. Finally, \mathbf{n}_1^*
 450 and \mathbf{n}_2^* are computed from \mathbf{m}^* . In this way a realization $\mathbf{p}^* = [\mathbf{m}^*, \mathbf{n}_1^*, \mathbf{n}_2^*, \mathbf{n}_3^*]$ of
 451 $\rho_C(\mathbf{p})$ is generated. 11 independent realizations of $\rho_C(\mathbf{p})$ are shown in Figure 1b.

452 $\rho_C(\mathbf{p})$ is designed to reflect available information related to the subsurface at Mor-
 453 rill (Abraham et al., 2012; Hansen & Minsley, 2019). $\rho_A(\mathbf{p})$ and $\rho_B(\mathbf{p})$ are considered
 454 here to investigate how the proposed methodology reacts to a uniform (maximum en-
 455 tropy) prior such as $\rho_A(\mathbf{p})$, and a simple prior as $\rho_B(\mathbf{p})$.

456 3.2.3 Noise

457 The noise of the EM data is assumed to be independent uncorrelated zero-mean
 458 Gaussian noise, with a standard deviation of 5 ppm (parts per million) plus 5 percent
 459 noise relative to the noise-free data value. This is the same noise model as considered
 460 in previous works on the EM data from Morrill (B. J. Minsley, 2011; Hansen & Mins-
 461 ley, 2019; Hansen, 2021).

462 3.3 Sampling of the posterior distribution

463 For reference, the extended rejection sampler, with a lookup table of size $N_T =$
 464 $2 \cdot 10^6$, is used to sample the posterior distribution, as detailed in Hansen (2021). 11 in-
 465 dependent realizations of the three posterior distributions ($\sigma_A(\mathbf{p})$, $\sigma_B(\mathbf{p})$, and $\sigma_C(\mathbf{p})$) are
 466 shown in Figures 1b,d,f.

467 The goal of the proposed machine learning approach is to directly compute statisti-
 468 cal properties of the posterior distribution similar to obtaining the same statistical prop-
 469 erties from a sample of the posterior obtained using sampling, such as shown in Figures
 470 1b,d,f.

471 3.4 Neural network design

472 Two fully connected neural networks are designed to allow characterizing the 1D
 473 marginal posterior distribution of continuous and discrete parameters. The input layer,
 474 in both cases, consists of the observed data \mathbf{d}_{obs} , or simulated data with noise. For this
 475 specific case, it consists of 12 neurons.

476 The inner network is designed using a number of hidden layers, each with 40 neu-
 477 rons with the Exponential Linear Unit (ELU) activation function (Bishop et al., 1995).
 478 This inner part of the network should be complex enough that the desired mapping can

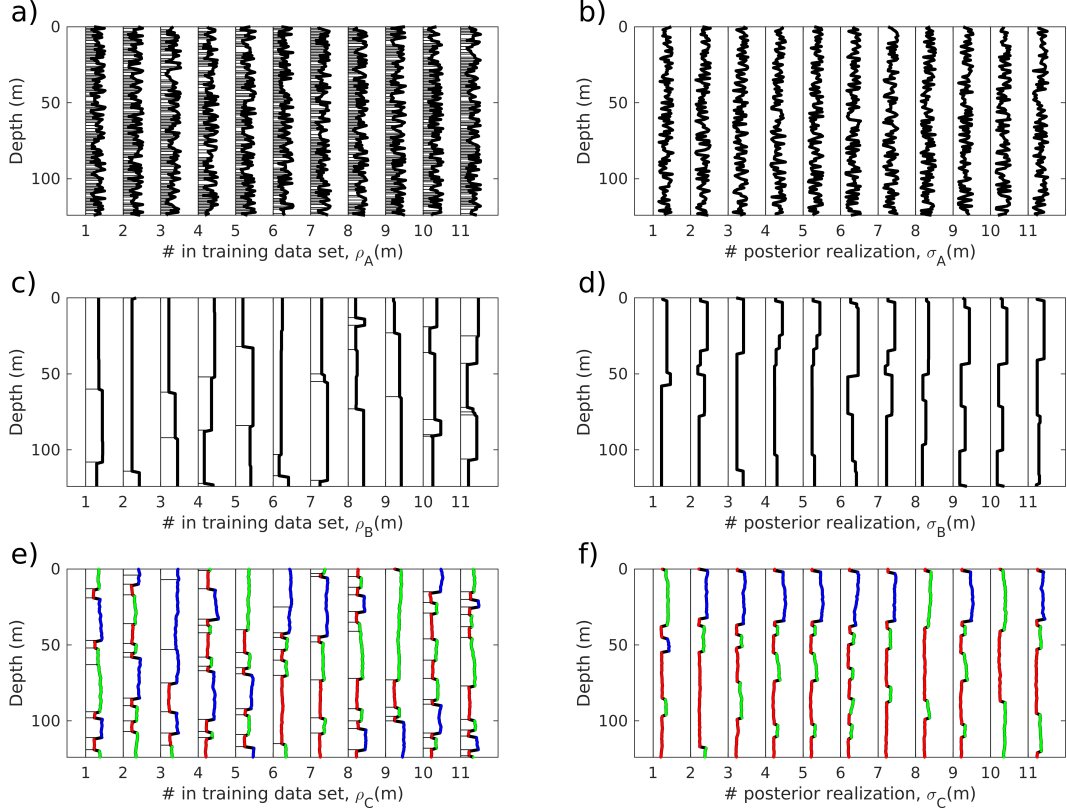


Figure 1. First 11 models from the lookup table for three prior models a) $\rho_a(\mathbf{m}, \mathbf{n}_1)$, c) $\rho_b(\mathbf{m}, \mathbf{n}_1)$, and e) $\rho_c(\mathbf{m}, \mathbf{n}_1, \mathbf{n}_2)$, as well as 11 independent realizations from the posterior distribution obtained for the data at $x=15\text{km}$ for a) $\sigma_a(\mathbf{m}, \mathbf{n}_1)$, c) $\sigma_b(\mathbf{m}, \mathbf{n}_1)$, and e) $\sigma_c(\mathbf{m}, \mathbf{n}_1, \mathbf{n}_2)$. Thin black lines indicate the existence of a layer interface (\mathbf{n}_1). The thick line indicates variation in resistivity (\mathbf{m}). In c) the colors of the thick line represent lithology A (red), B (blue), and C (green) when defined.

479 be represented, but simple enough to avoid overfitting, as discussed also by (Meier et al.,
 480 2007). Network design is highly problem-dependent, and for the present problem, we found
 481 this network design provides results on par with, and in some cases better than, sampling-
 482 based approaches, while at the same time being relatively easy to optimize.

483 The choice of loss function, and to some extent the activation function, defines the
 484 specific property of the posterior distribution that will be estimated. This leads to two
 485 specific types of output layers for regression and classification type problems¹.

486 **3.4.1 Regression type neural network**

487 The first neural network type is designed to estimate parameters θ of a probabil-
 488 ity distribution describing the 1D marginal posterior distribution of a continuous param-
 489 eter (such as \mathbf{m} and \mathbf{n}_3). If N_θ is the number of parameters needed to describe a spe-
 490 cific 1D distribution, then in total $N_{out} = N_\theta N_m$ neurons are needed in the output layer
 491 if the target is properties of $\sigma(\mathbf{m})$, and $N_{out} = N_\theta$ if the target is $\sigma(\mathbf{n}_3)$.

492 **3.4.2 Classification type neural network**

493 The second neural network type is designed to estimate the posterior probability
 494 of possible classes for the discrete type model parameters \mathbf{n}_1 and \mathbf{n}_3 , i.e. of $\sigma(\mathbf{n}_1)$ $\sigma(\mathbf{n}_3)$.

495 If the goal is to estimate the 1D marginal distribution of a discrete parameter with
 496 N_{cat} possible outcomes, this can be achieved by selecting an output layer with $N_{out} =$
 497 N_m when $N_{cat} = 2$ (using a sigmoid activation function), and $N_{out} = N_{cat} N_m$ when
 498 $N_{cat} > 2$ (using the softmax activation function). As discussed above, using the cross-
 499 entropy loss function, Eqn. 17, will lead to direct estimation of the 1D posterior marginal
 500 probabilities in this case.

501 **3.5 Network training**

502 Using the nonlinear forward model and the noise model, a training data set of size
 503 $N_T = 1000000$ is constructed (one for each type of prior model) and used for training.
 504 Both networks are trained using 67% of the training data set, while 33% is reserved for
 505 validation. In both cases, the loss function is minimized using the Adam optimizer (Kingma
 506 & Ba, 2014) using a learning rate of 0.001, for a maximum of 2000 epochs. Early stop-
 507 ping is utilized which stops the training if the loss function evaluated on the validation
 508 data does not decrease for 50 epochs. This is done to avoid over-fitting, where the loss
 509 on the training data will decrease, but where the loss on the validation data increases.
 510 TensorFlow with Keras and TensorFlow-probability have been used to implement and
 511 train the neural networks (Abadi et al., 2015; Chollet, 2015; Dillon et al., 2017).

512 The two considered networks, and the training of the networks, only differ concern-
 513 ing the definition of the output layer (the number of nodes and activation function), the
 514 choice of loss function, and the chosen number of hidden layers.

515 **3.6 Estimation of properties of $\sigma(\mathbf{m})$**

516 First, properties related to the posterior distribution of resistivity, $\sigma(\mathbf{m})$, are con-
 517 sidered.

¹ Example implementations of these two types of neural networks can be found at http://github.com/cultpenguin/ip_and_ml/.

518

3.6.1 Estimation of mean and standard deviation of $\sigma(\mathbf{m})$

519

520

521

A neural network is set up and trained to estimate the pointwise mean and standard deviation of $\sigma(\mathbf{m})$, using 8 hidden layers, by minimizing the loss function in Eqn 13.

522

523

524

525

526

527

Figures 2a-d shows the pointwise mean of the posterior distribution $\sigma_C(\mathbf{m})$ obtained using the machine learning approach with a training data set of size $N = [1000, 10000, 100000, 1000000]$, compared to the same statistics computed from a sample of the posterior obtained using the sampling method, Figure 2e. The corresponding standard deviation controls the transparency in the plot, with high transparency corresponding to high standard deviation²

528

529

530

531

It is clear from Figure 2a that using $N_T = 1000$ provides very poor results, as compared to the results obtained using sampling, Figure 2e. But even using $N_T = 10000$ leads to results close to the sampling-based results. For $N_T \geq 100000$ the quality of the direct estimates of the mean and standard deviation does not seem to differ much.

532

533

534

535

536

537

One notable difference when comparing Figure 2d ($N_T=1000000$) and 2e (sampling), is that sampling results in more small scale variability in the estimated parameters, as opposed to the more smooth result obtained using machine learning. The reason is simply that the sampling-based approach is based on inferring the statistics from a finite-sized sample of the posterior, whereas in the machine learning approach these statistics are estimated directly.

538

539

540

541

Figure 3 shows a comparison between the posterior mean (with standard deviation used to control transparency) obtained using the sampling approach and using the machine learning approach ($N_T = 1000000$), for $\sigma_A(\mathbf{m})$ (Figures 3a-b) and $\sigma_B(\mathbf{m})$ (Figures 3c-d) respectively.

542

543

544

545

$\rho_A(\mathbf{m})$ refers to the least informed prior model, and hence one should expect the least resolution in the corresponding posterior distribution. This is what can be seen in results from both the machine learning and the sampling approach, Figures 3a-b, where only the top high resistive layer is somewhat resolved.

546

547

548

549

While $\rho_B(\mathbf{m})$ is somewhat simpler than $\rho_C(\mathbf{m})$, the mean and standard deviation of the corresponding posterior distribution are rather similar, with most difference related to the posterior standard deviation (as illustrated by the transparency in Figures 2 and 3c-d).

550

551

552

553

A key point from Figures 2 and 3 is that the use of the machine learning based approach seems to provide results at least on par with the results obtained using sampling, when the goal is to estimate the mean and standard deviation of the (non-Gaussian) posterior distribution. This is the case using both informed and uninformed prior models.

554

555

556

557

558

559

560

3.6.1.1 Computational efficiency Figure 4 shows the computation time³ needed to train the neural networks for the results presented in Figure 2. The training time increase with the size of the training data set, N_T . Both training and validation loss is reduced when N_T increases. It is also clear that the relative difference in loss decreases when comparing the use of $N_T = 100000$ to $N_T = 1000000$, to when comparing the use of $N_T = 1000$ to $N_T = 10000$. Hence, using $N_T > 100000$ leads to a substantial longer training time, but only to a minor loss reduction.

² The mean and standard deviation without transparency are available in the supplementary material.

³ a workstation with an Intel Core(TM) i7-8700K CPU, Nvidia RTX 3090 GPU, and 64 Gb RAM was used

561 Once set up and trained, the prediction of the network is very fast. For all the net-
 562 works presented above, the prediction time for all 451 data locations was less than 5ms.
 563 This means that more than 100000 soundings can be analyzed per second.

564 **3.6.2 Estimation of multiple 1D properties of $\sigma(m_i)$**

565 As described above, any parameter of a probability distribution for which a loss
 566 function can be described through Eqn. 10 can be estimated using the machine learn-
 567 ing method. To demonstrate this, 4 independent networks have been trained to estimate
 568 properties (Θ) of the 1D marginal posterior distribution $\sigma(m_i)$ given by a) a normal dis-
 569 tribution (Eqn. 11, as in Figure 2), b) a generalized normal distribution (Eqn. 14), c)
 570 a mixture distribution based on two Gaussian distributions (Eqn. 14), and d) a mixture
 571 distribution based on three Gaussian distributions (Eqn. 14). The loss functions used
 572 are the negative log-likelihood of the probability distribution in Eqns. 11, 14, and 15 re-
 573 spectively.

574 The number of parameters to estimate for the 4 cases, and hence neurons in the
 575 output layer, is $N_\theta = [2*N_m, 3*N_m, 2*N_m*N_c, 3*N_m*N_c] = N_\theta = [250, 375, 750, 1125]$,
 576 where N_c is the number of distributions in the mixture model.

577 Figure 5a shows the posterior 1D marginal distribution of resistivity values obtained
 578 using sampling, based on a finite set of realizations, obtained at $x=15$ km. One can clearly
 579 identify a bimodal to trimodal distribution at depth representing the three possible litholo-
 580 gies from the prior model $\rho_C(\mathbf{m})$ with different resistivity values.

581 Figures 5b-f, shows the probability distributions representing the estimated sta-
 582 tistical properties of the 4 considered distributions. These distributions do not represent
 583 assumptions about the posterior distribution (which can be arbitrarily complex) but re-
 584 flect the statistical properties one would get if the particular choice of distribution is used
 585 to represent a sample of the posterior.

586 If the goal is to compute a representation of the 1D posterior marginal distribu-
 587 tion, as considered by (Meier et al., 2007; Shahraeeni & Curtis, 2011), then care should
 588 be taken to use a parameterizations for the chosen 1D distribution complex enough to
 589 allow describing the variability of the posterior. From Figure 5 it is evident that only
 590 in case using the mixture model with 3 Gaussian distributions, the estimated marginal
 591 probability density represents the actual 1D marginal posterior distribution well.

592 The statistical parameters of the posterior distribution which it is relevant to com-
 593 pute for a specific inverse problem, is naturally problem-dependent. This example nonethe-
 594 less demonstrates that the machine learning methodology is capable of estimating pa-
 595 rameters of different types of probability distributions, for which a probability density,
 596 and hence the corresponding loss function, can be computed.

597 **3.7 Estimation of properties of $\sigma(\mathbf{n}_2)$**

598 We consider the simpler problem of inferring information about a single continu-
 599 ous parameter, \mathbf{n}_2 , representing the cumulative thickness of layers with a resistivity above
 600 225 ohmm. The same neural network is used as considered above to estimate proper-
 601 ties related to \mathbf{m} , except here only 4 hidden layers are used.

602 Figure 6 shows the mean of $\sigma_C(\mathbf{n}_2)$ (black line), as well as the probability distri-
 603 bution reflecting the mean and standard deviation estimated using the machine learn-
 604 ing approach for $N_T = [1000, 10000, 100000, 1000000]$ in figures 6a-d. The mean com-
 605 puted using the machine learning approach compares well to the mean obtained using
 606 sampling methods for $N_T \geq 100000$.

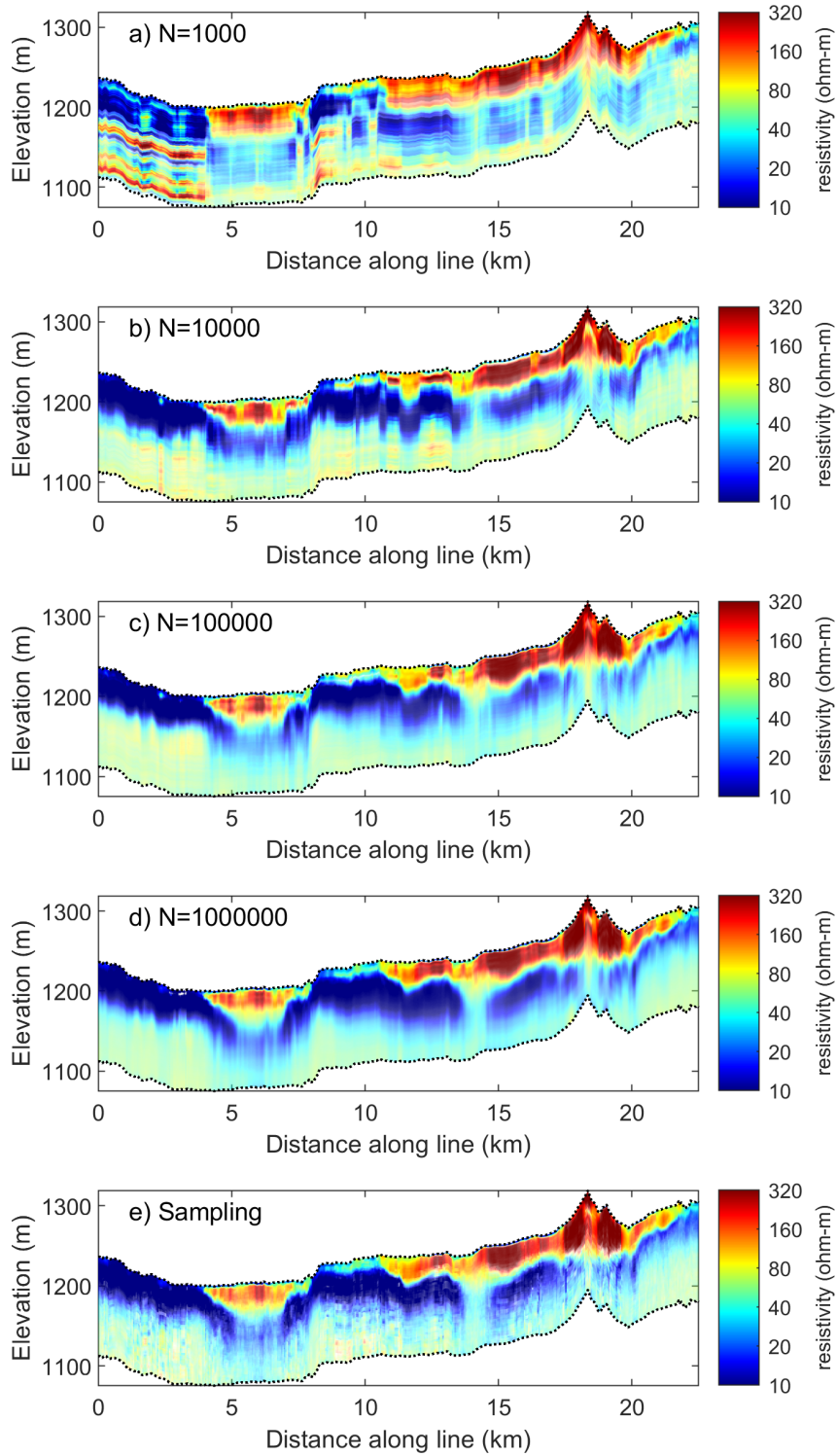


Figure 2. Pointwise mean obtained from $\sigma_C(\mathbf{m})$ obtained using machine learning based on a training data set of size a) 1000, b) 10000, c) 100000, and d) 1000000, and using e) the extended rejection sampler. Transparency based on pointwise posterior standard deviation. The mean and standard deviation without transparency are available in the supplementary material.

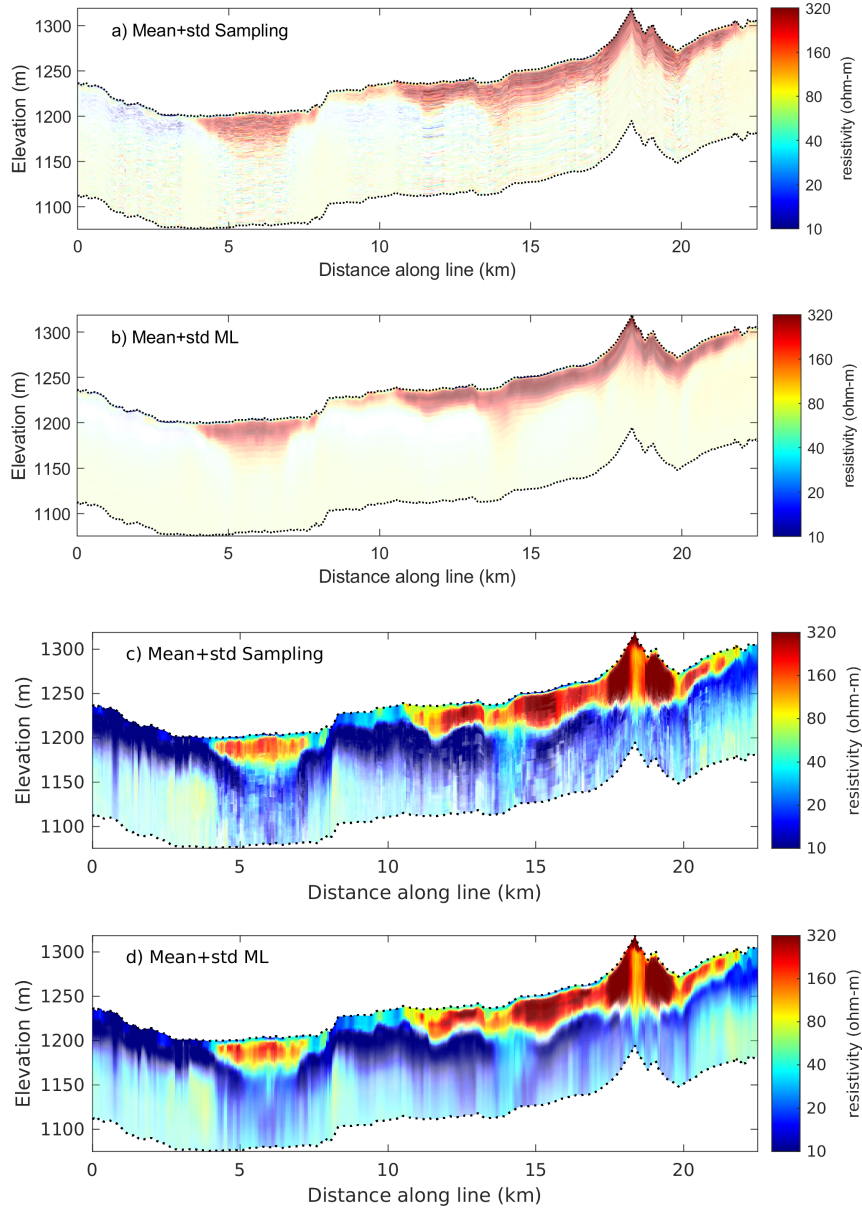


Figure 3. a-b) Pointwise mean obtained from $\sigma_A(\mathbf{m})$ obtained using the extended rejection sampler (a) and machine learning (b) based on a training data set of size 1000000. c-d) As a-b) but for $\sigma_B(\mathbf{m})$. Transparency based on pointwise posterior standard deviation. The mean and standard deviation without transparency are available in the supplementary material.

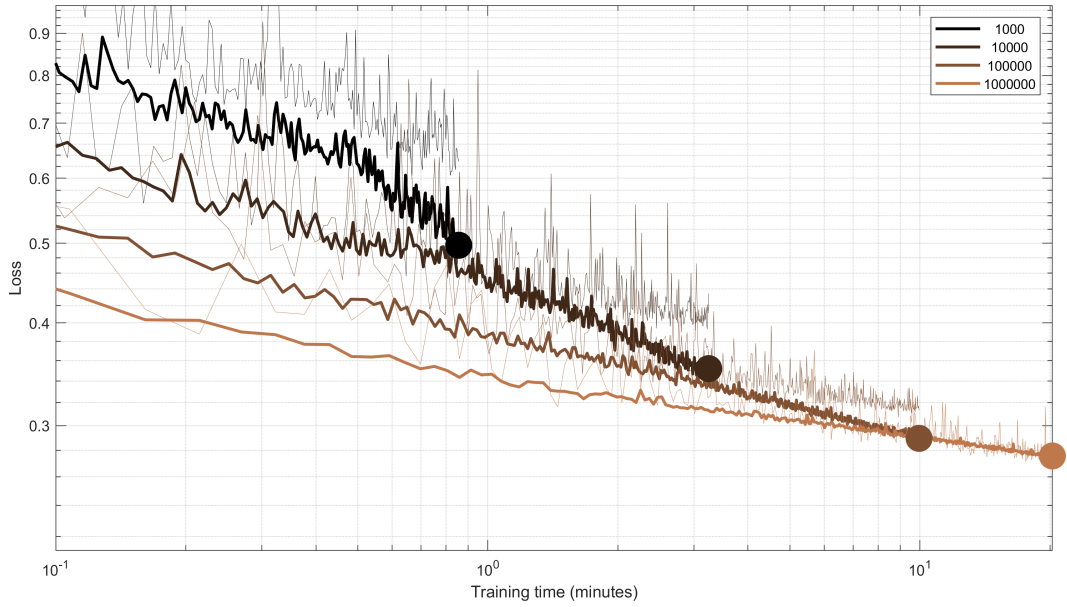


Figure 4. Training (thick lines) and validation (thin lines) loss as a function of training time for $N_t = [1000, 10000, 100000, 1000000]$.

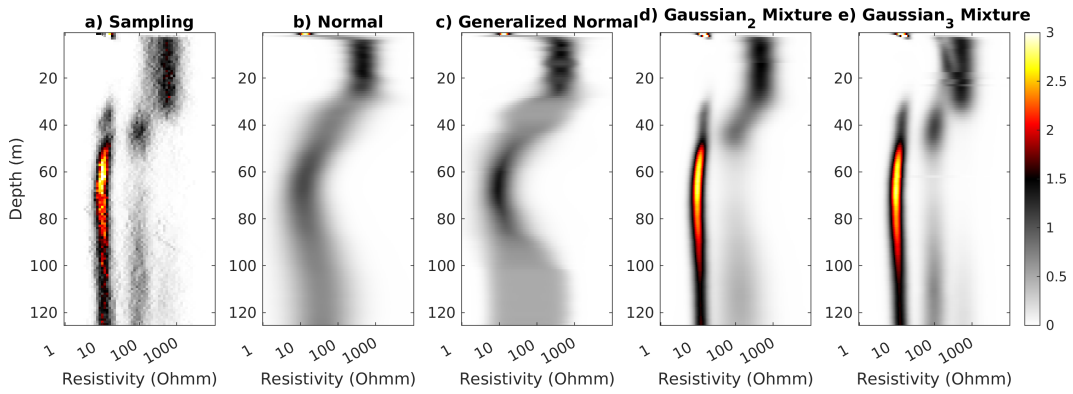


Figure 5. 1D posterior probability density with depth using data at $X=6.2$ km a) obtained using sampling, and constructed from statistical properties inferred for b) normal distribution, c) generalized normal distribution, d)-e) a mixture model based on 2 and 3 1D normal distributions.

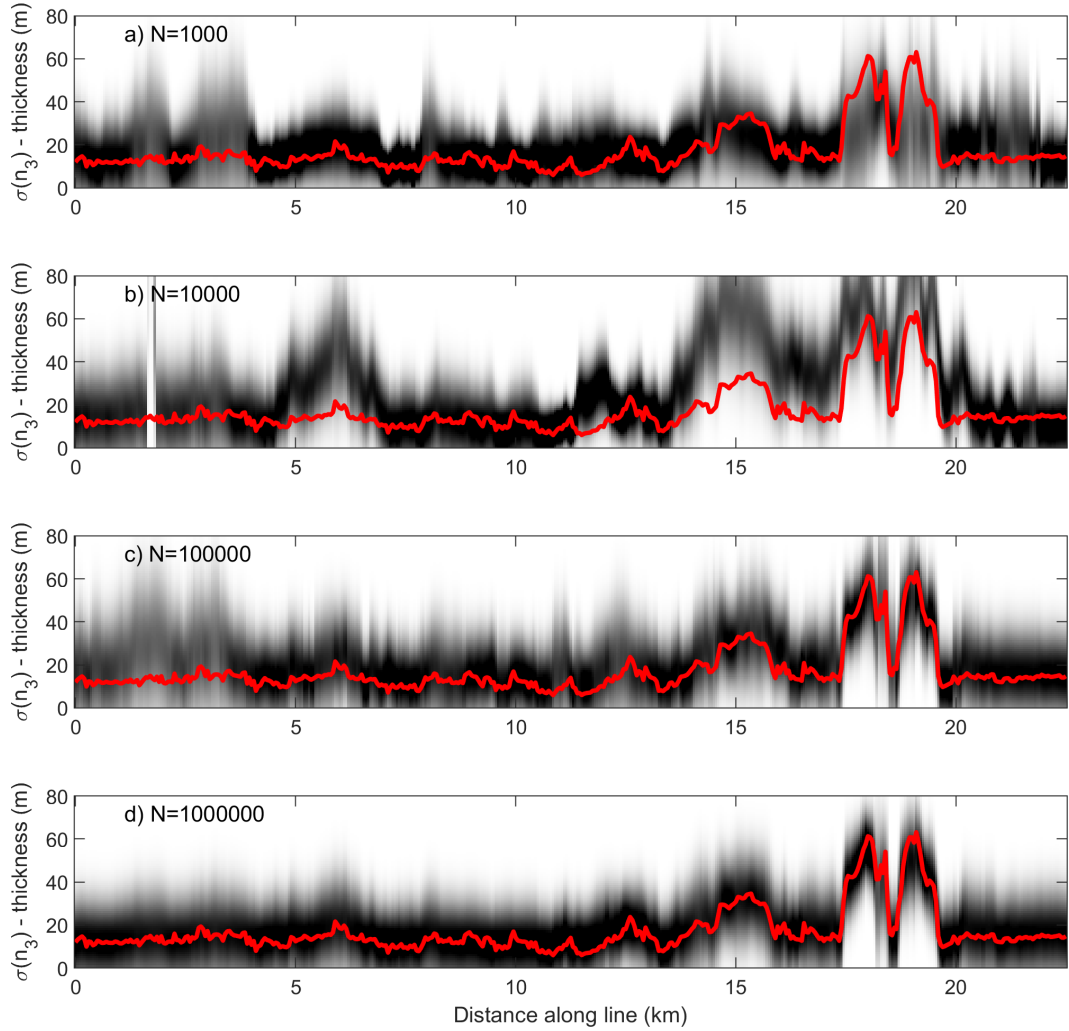


Figure 6. Mean of the posterior distributions $\sigma_C(\mathbf{n}_3)$ estimated using sampling (red line) compared with the estimated mean and standard deviation of $\sigma_C(\mathbf{n}_3)$ (probability density as grayscale) estimated using the machine learning approach using a training data set of size $N_T = [1000, 10000, 100000, 1000000]$ in a)-d).

607 3.8 Estimation of properties of $\sigma(\mathbf{n}_1)$

608 $\sigma(\mathbf{n}_1)$ refers to the existence (or lack of) a layer interface, which can be formulated
 609 as a binary classification problem. Therefore, a classification type network is constructed
 610 using a sigmoid activation function, and the loss function in Eqn. 17. 4 hidden layers
 611 are used.

612 Figures 7a and 7c refer to the pointwise posterior probability of locating a layer
 613 interface, as computed from a sample from the posterior distribution of $\sigma_B(\mathbf{n}_1)$ and $\sigma_C(\mathbf{n}_1)$.
 614 The corresponding results obtained as the output of a trained neural network based on
 615 a training data set of size $N_T = 1000000$ are shown in Figures 7b and 7d. The prior
 616 probability of a layer interface is around 0.1, and hence a posterior probability of 0.25
 617 is indicative of a layer interface.

618 The results using sampling and the machine learning approach are in both cases
 619 very similar with a bit more variability in the results obtained using sampling, due to
 620 the use of a finite-sized sample of the posterior distribution.

621 3.9 Estimation of properties of $\sigma(\mathbf{n}_3)$

622 Finally, we consider the discrete parameter \mathbf{n}_3 which refer to lithology type, which
 623 can be of type '1', '2' and '3'. The outcome at each model parameter is then a multi-
 624 class (three classes) classification problem. Therefore, a classification type network is con-
 625 structed using a softmax activation function, and the loss function in Eqn. 17. 4 hid-
 626 den layers is used.

627 Figures 8a,c,e show the posterior probability for each of the three classes obtained
 628 using sampling, while Figures 8b,d,f show the corresponding results obtained by eval-
 629 uating the trained network. Except for some small-scale variations in the sampling re-
 630 sults, due to using finite sample size, the obtained posterior statistics are strikingly sim-
 631 ilar.

632 4 Discussion

633 A typical application of probabilistic inversion is to use some sampling method to
 634 generate a large sample from the posterior distribution. Then some appropriate statis-
 635 tic, computed from the sample of the posterior distribution, is chosen and visualized.

636 The theory presented above proposes how one can construct a neural network that
 637 can directly estimate any statistical property of the posterior distribution (for discrete
 638 and continuous parameters) for which a probability distribution can be evaluated, with-
 639 out ever generating realizations of the posterior distribution. This can be achieved by

- 640 1. Construct a training data set, in the style of Devilee et al. (1999), $\mathbf{T}^* = [\mathbf{N}^*, \mathbf{D}_{sim}^*]$,
 641 where \mathbf{N}^* represents a set of features/properties of interest, and \mathbf{D}_{sim}^* represents
 642 a corresponding set of simulated data with noise, using both the forward and the
 643 noise model.
- 644 2. Design a neural network whose output layer represents the relevant statistical pa-
 645 rameters Θ of the posterior distribution $\sigma(\mathbf{n})$ of interest.
- 646 3. Train the neural network by minimizing a loss function that is the negative log-
 647 likelihood of the probability density, $f(\Theta)$, whose properties one wishes to esti-
 648 mate.

649 Practical application of the methodology requires a) a neural network structure complex
 650 enough to be able to estimate the mapping $\mathbf{d}_{sim} \mapsto \Theta$, and b) a training data set large
 651 enough to allow inferring the mapping.

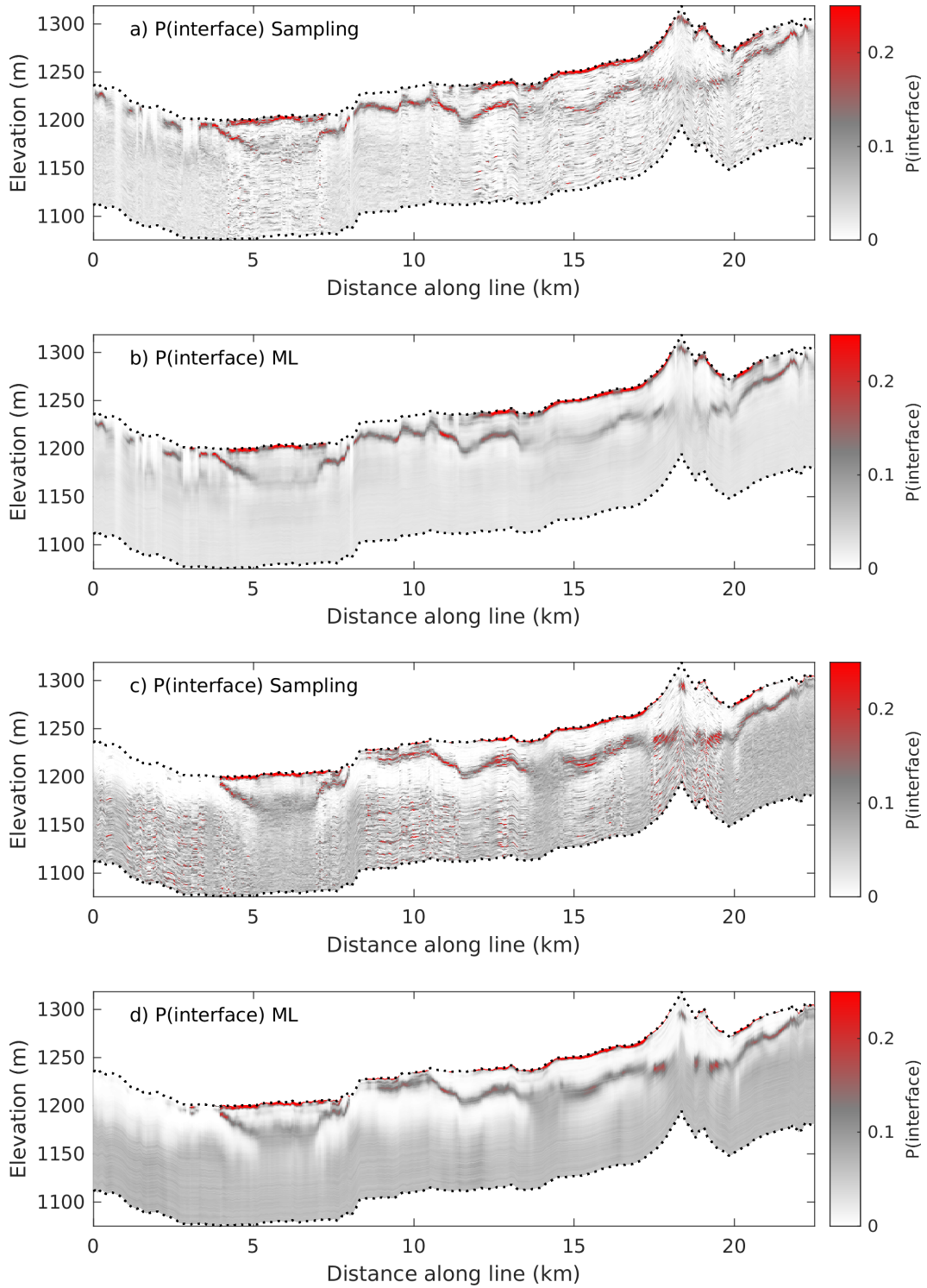


Figure 7. a-b) Posterior probability of a layer interface obtained using extended rejection sampling (a), and machine learning (b), for $\sigma_B(\mathbf{n}_1)$. c-d) Posterior probability of a layer interface obtained using extended rejection sampling (c), and machine learning (d), for $\sigma_C(\mathbf{n}_1)$.

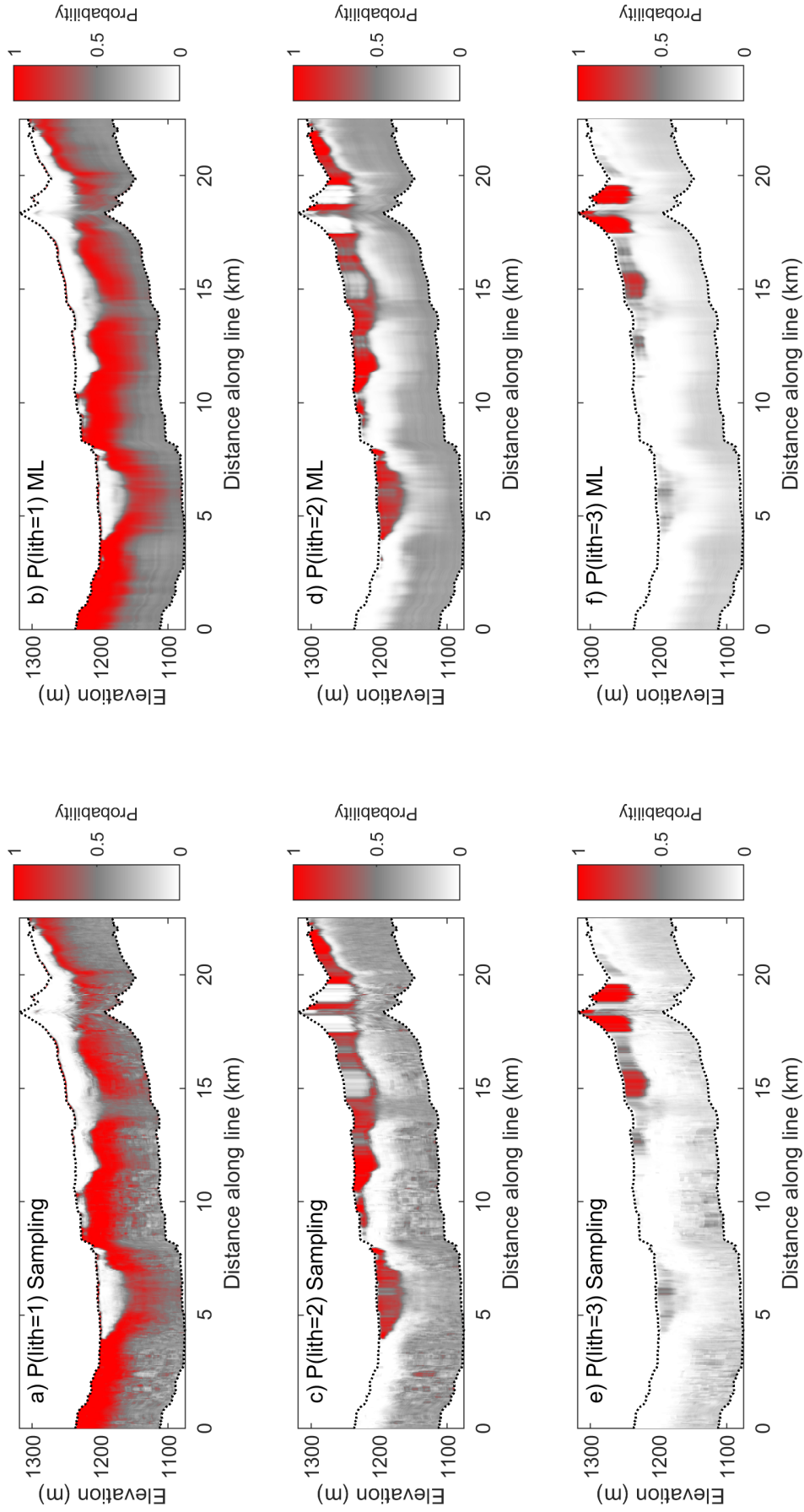


Figure 8. Posterior probability of lithology, using a-c) sampling and d-f) machine learning for $\sigma_C(\mathbf{n}_3)$.

652 The methodology was applied and demonstrated in a case study using airborne EM
 653 data from Morrill, Nebraska. Several (uninformed to more informed) prior models were
 654 considered, describing both subsurface resistivity (a continuous parameter, \mathbf{m}) and lithol-
 655 ogy (a discrete parameter, \mathbf{n}_2) and the considered forward problem was nonlinear. In
 656 addition, the method was used to estimate posterior statistics of low-dimensional fea-
 657 tures of the prior models, such as the existence of a layer interface, \mathbf{n}_1 , and the thick-
 658 ness of layers with resistivity above 225 ohmm, \mathbf{n}_3 . Results showed that using a train-
 659 ing data set of size $N_T \geq 100000$ leads to a trained neural network that provides es-
 660 timates of posterior statistics similar to those obtained using sampling methods, using
 661 a fraction of the computational power (about 5ms per sounding).

662 **Relation to previous work**

663 The methodology proposed here is based on the ideas originally proposed by Devilee
 664 et al. (1999) and extended by e.g. Meier et al. (2007); Earp et al. (2020). The explicit
 665 goal of Meier et al. (2007), and following related work (Shahraeeni & Curtis, 2011; de
 666 Wit et al., 2013; Earp et al., 2020), is to model the marginal posterior distribution as
 667 a mixture of Gaussian distributions.

668 The key goal of this manuscript is to show that one can construct a neural network
 669 that can estimate any desired statistical parameter describing the posterior distribution
 670 $\sigma(\mathbf{m}, \mathbf{n})$ related to both the main set of model parameters \mathbf{m} and any set of parameters
 671 \mathbf{n} related to the main parameters, for which an appropriate loss function can be defined.
 672 Such statistical parameters can, as a special case, represent the 1D marginal posterior
 673 distribution (as shown in Figure 5e) as in Meier et al. (2007).

674 **Limitations**

675 The proposed method does not generate realizations of the posterior distribution,
 676 as do other sampling-based methods (B. J. Minsley, 2011; Brodie & Sambridge, 2012;
 677 Hansen & Minsley, 2019; Hansen, 2021). Instead, statistics of the posterior distribution
 678 of features of interest are estimated directly by applying a trained neural network.

679 In some use cases, one may need the realizations, for example to propagate flow
 680 responses from of a set of realizations from the posterior representing hydraulic param-
 681 eters, (Vilhelmsen et al., 2019). But, in many applications, where one is primarily in-
 682 terested in some statistical parameter describing the posterior, such as the posterior prob-
 683 ability of a lithology type, the presented methodology may be very useful.

684 The methodology is particularly promising for localized inverse problems, where
 685 the trained neural network can be set up and trained once, but applied many times. It
 686 is less obviously suited to 3D inversions with very large model dimensions because 1) con-
 687 struction an adequately large training data set will be difficult and CPU intensive, 2)
 688 solving the 3D forward problem may be CPU intensive, and 3) it may be very difficult
 689 to train a neural network with millions of parameters in the output layer. The use of vari-
 690 ational inference has been suggested as a more efficient approach to estimate marginal
 691 statistics for higher dimensional inverse problems, see e.g. Zhang and Curtis (2020a).

692 **Potential**

693 The immediate appeal of the proposed methodology is that it leads to fast predic-
 694 tion times. One can get similar results, but much faster, compared with using sampling-
 695 based methods to analyze the posterior distribution.

696 The presented method is faster than linearized least squares based deterministic
 697 inversion of EM data (Auken et al., 2017), which have been widely used for inversion of
 698 large surveys (B. Minsley et al., 2021) because they require much less computational re-

699 sources than sampling-based methods. With the computational efficiency of the proposed
 700 method, the computational benefits of linearized methods are no longer so substantial
 701 that one should ignore the benefits of using the probabilistic methods that allow the use
 702 of site-specific prior information, a non-linear forward model, and full exploration of the
 703 space of uncertainty.

704 The more general appeal is that the proposed methodology allows the use of in prin-
 705 ciple arbitrarily complex prior models. The only requirement is that one must be able
 706 to generate independent realizations of the prior model. This allows an end-user to ac-
 707 tively choose a prior model based on available information, as opposed to being forced
 708 to use the implicit prior assumptions in most available inversion algorithms, such as the
 709 assumptions of a layered subsurface (B. J. Minsley, Foks, & Bedrosian, 2021) or a Gaus-
 710 sian type smooth prior (Auken & Christiansen, 2004). The prior can be constructed ac-
 711 cording to site-specific information, and can then estimate posterior statistics of any pa-
 712 rameter that can be computed from the prior model, as illustrated with the parameters
 713 \mathbf{n}_1 and \mathbf{n}_2 in the case study

714 The main challenge then becomes the construction of realistic prior models that
 715 represent geological realistic information.

716 *Workflow for decision makers.*

717 A key feature/limitation of the proposed methodology is that a realization of the
 718 posterior is never realized. Instead, statistics of features of the posterior distribution are
 719 computed directly.

720 We argue that for decision-makers it is the statistics of features related to model
 721 parameters that are most often of interest, not the individual realizations themselves,
 722 as discussed by Scales and Snieder (1997). Even if a large sample exists of the posterior
 723 distribution for each data location along the considered profile of data at Morrill, then
 724 one will have to compute some feature/statistics of this sample to make it useable by decision-
 725 makers.

726 The examples presented here demonstrate that similar results are obtained using
 727 either sampling of the posterior distribution, followed by analyses of the sample of the
 728 posterior distribution, or directly using the proposed machine learning methodology. The
 729 key practical difference to using sampling methods is then that with our proposed method-
 730 ology one has to quantify the feature that one is interested in and specify an appropri-
 731 ate loss function before running the inversion. Whereas using sampling methods to sam-
 732 ple the posterior, one can convert the realizations of the posterior into a specific feature,
 733 and perform the posterior analysis, after the sampling algorithm has run.

734 **5 Conclusions**

735 A simple, yet powerful, approach to probabilistic inversion has been proposed. Its
 736 application requires that one can simulate sets of examples capturing the known infor-
 737 mation. That is 1) sample from an arbitrarily complex prior model, 2) solving the for-
 738 ward problem, and 3) adding realistic noise to the simulated data. From each of these
 739 sets of models and data, a set of corresponding features related to the model paramet-
 740 ers can be obtained. Together these represent, up to the limit of the finite set of mod-
 741 els, all known information about these features of interest.

742 From such sets of features and corresponding noisy input data, posterior statistics
 743 describing the features given the data can be obtained by minimizing an appropriate loss
 744 function. This provides the ability to carry out a fast and accurate estimation of rele-
 745 vant posterior statistics given an observed dataset.

746 A case study of the methodology applied to a nonlinear probabilistic inversion of
 747 EM data demonstrates it is possible to obtain posterior statistics similar to those obtained
 748 using sampling methods, using a fraction of the computation time. This approach al-
 749 lows the use and testing of multiple prior models, and to consider multiple features re-
 750 lated to the prior distributions, in a fully probabilistic setting using only modest com-
 751 putational resources. The method has most appeal for localized inverse problems, where
 752 the same trained neural network can be applied on many datasets with little computa-
 753 tional effort.

754 Data Availability Statement

755 The airborne EM data used in this study is freely available (Smith et al., 2010) and
 756 can be accessed through <https://doi.org/10.3133/ofr20101259>. Training data sets
 757 and python notebooks for training and prediction will be made available upon publica-
 758 tion at https://github.com/cultpenguin/probabilistic-inverse-problems_and_ml

759 Acknowledgments

760 This work is funded by the Danish Free Research Council, project 717-00160B.

761 References

- 762 Abadi, M., Agarwal, A., Barham, P., Brevdo, E., Chen, Z., Citro, C., ... Zheng, X.
 763 (2015). *TensorFlow: Large-scale machine learning on heterogeneous systems*.
 764 Retrieved from <https://www.tensorflow.org/> (Software available from
 765 tensorflow.org)
- 766 Abraham, J. D., Cannia, J. C., Bedrosian, P. A., Johnson, M. R., Ball, L. B., &
 767 Sibray, S. S. (2012). *Airborne electromagnetic mapping of the base of aquifer*
 768 *in areas of western nebraska*. U.S. Geological Survey Scientific Investigations
 769 Report 2011-5219, 38 p.
- 770 Ardizzone, L., Kruse, J., Wirkert, S., Rahner, D., Pellegrini, E. W., Klessen, R. S.,
 771 ... Köthe, U. (2018). Analyzing inverse problems with invertible neural
 772 networks. *arXiv preprint arXiv:1808.04730*.
- 773 Auken, E., Boesen, T., & Christiansen, A. V. (2017). A review of airborne elec-
 774 tromagnetic methods with focus on geotechnical and hydrological applications
 775 from 2007 to 2017. *Advances in Geophysics*, 58, 47–93.
- 776 Auken, E., & Christiansen, A. V. (2004). Layered and laterally constrained 2d inver-
 777 sion of resistivity data. *Geophysics*, 69(3), 752–761.
- 778 Auken, E., Christiansen, A. V., Kirkegaard, C., Fiandaca, G., Schamper, C.,
 779 Behroozmand, A. A., ... others (2014). An overview of a highly versatile
 780 forward and stable inverse algorithm for airborne, ground-based and borehole
 781 electromagnetic and electric data. *Exploration Geophysics*, 46(3), 223–235.
- 782 Bai, P., Vignoli, G., Andrea, V., Jouni, N., & Vacca, G. (2020). (quasi-) real-time
 783 inversion of airborne time-domain electromagnetic data via artificial neural
 784 network. *Remote Sensing*.
- 785 Bishop, C. M., et al. (1995). *Neural networks for pattern recognition*. Oxford univer-
 786 sity press.
- 787 Blei, D. M., Kucukelbir, A., & McAuliffe, J. D. (2017). Variational inference:
 788 A review for statisticians. *Journal of the American statistical Association*,
 789 112(518), 859–877.
- 790 Bording, T. S., Asif, M. R., Barfod, A. S., Larsen, J. J., Zhang, B., Grombacher,
 791 D. J., ... others (2021). Machine learning based fast forward modelling of
 792 ground-based time-domain electromagnetic data. *Journal of Applied Geo-*
 793 *physics*, 104290.
- 794 Bosch, M., Mukerji, T., & Gonzalez, E. F. (2010). Seismic inversion for reservoir

- 795 properties combining statistical rock physics and geostatistics: A review. *Geo-*
796 *physics*, 75(5), 75A165–75A176.
- 797 Brodie, R. C., & Sambridge, M. (2012). Transdimensional Monte Carlo inversion of
798 AEM data. *ASEG Extended Abstracts*, 2012(1), 1–4.
- 799 Chollet, F. (2015). *Keras*. <https://github.com/fchollet/keras>. GitHub.
- 800 Christensen, N. B. (2002). A generic 1-D imaging method for transient electromag-
801 netic data. *Geophysics*, 67(2), 438–447.
- 802 Constable, S. C., Parker, R. L., & Constable, C. G. (1987). Occam’s inversion: A
803 practical algorithm for generating smooth models from electromagnetic sound-
804 ing data. *Geophysics*, 52(3), 289–300.
- 805 Conway, D., Alexander, B., King, M., Heinson, G., & Kee, Y. (2019). Inverting
806 magnetotelluric responses in a three-dimensional earth using fast forward ap-
807 proximations based on artificial neural networks. *Computers & geosciences*,
808 127, 44–52.
- 809 Cox, L. H., Wilson, G. A., & Zhdanov, M. S. (2010). 3D inversion of airborne elec-
810 tromagnetic data using a moving footprint. *Exploration Geophysics*, 41(4),
811 250–259.
- 812 Devilee, R., Curtis, A., & Roy-Chowdhury, K. (1999). An efficient, probabilistic
813 neural network approach to solving inverse problems: inverting surface wave
814 velocities for eurasian crustal thickness. *Journal of Geophysical Research: Solid*
815 *Earth*, 104(B12), 28841–28857.
- 816 de Wit, R. W., Valentine, A. P., & Trampert, J. (2013). Bayesian inference of
817 earth’s radial seismic structure from body-wave traveltimes using neural net-
818 works. *Geophysical Journal International*, 195(1), 408–422.
- 819 Dillon, J. V., Langmore, I., Tran, D., Brevdo, E., Vasudevan, S., Moore, D.,
820 ... Saurous, R. A. (2017). Tensorflow distributions. *arXiv preprint*
821 *arXiv:1711.10604*.
- 822 Earp, S., & Curtis, A. (2020). Probabilistic neural network-based 2d travel-time to-
823 mography. *Neural Computing and Applications*, 32(22), 17077–17095.
- 824 Earp, S., Curtis, A., Zhang, X., & Hansteen, F. (2020, 08). Probabilistic neural net-
825 work tomography across Grane field (North Sea) from surface wave dispersion
826 data. *Geophysical Journal International*, 223(3), 1741-1757. Retrieved from
827 <https://doi.org/10.1093/gji/ggaa328> doi: 10.1093/gji/ggaa328
- 828 Foks, N., & Minsley, B. (2020). *Geophysical Bayesian inference in Python (Geo-*
829 *BiPy)*. <https://github.com/usgs/geobipy>. GitHub. doi: 10.5066/P9K3YH9O
- 830 Geman, S., & Geman, D. (1984). Stochastic relaxation, gibbs distributions, and
831 the bayesian restoration of images. *IEEE Transactions on pattern analysis and*
832 *machine intelligence*(6), 721–741.
- 833 Grana, D., & Della Rossa, E. (2010). Probabilistic petrophysical-properties esti-
834 mation integrating statistical rock physics with seismic inversion. *Geophysics*,
835 75(3), O21–O37.
- 836 Grayver, A. V., Streich, R., & Ritter, O. (2013). Three-dimensional parallel dis-
837 tributed inversion of CSEM data using a direct forward solver. *Geophysical*
838 *Journal International*, 193(3), 1432–1446.
- 839 Green, P. J. (1995). Reversible jump Markov chain Monte Carlo computation and
840 Bayesian model determination. *Biometrika*, 82(4), 711–732.
- 841 Hansen, T. M. (2021). Efficient probabilistic inversion using the rejection sam-
842 pler—exemplified on airborne EM data. *Geophysical Journal International*,
843 224(1), 543–557.
- 844 Hansen, T. M., Cordua, K. C., & Mosegaard, K. (2012). Inverse problems with non-
845 trivial priors - efficient solution through sequential Gibbs sampling. *Computa-*
846 *tional Geosciences*, 16(3), 593-611. doi: 10.1007/s10596-011-9271-1
- 847 Hansen, T. M., & Cordua, K. S. (2017). Efficient monte carlo sampling of inverse
848 problems using a neural network-based forward—applied to gpr crosshole
849 travelttime inversion. *Geophysical Journal International*, 211(3), 1524–1533.

- 850 Hansen, T. M., Cordua, K. S., Jacobsen, B. H., & Mosegaard, K. (2014). Accounting
851 for imperfect forward modeling in geophysical inverse problems—exemplified
852 for crosshole tomography. *Geophysics*, *79*(3), H1–H21.
- 853 Hansen, T. M., Cordua, K. S., Looms, M. C., & Mosegaard, K. (2013, 03). SIPPI:
854 a Matlab toolbox for sampling the solution to inverse problems with com-
855 plex prior information: Part 1, methodology. *Computers & Geosciences*, *52*,
856 470–480. doi: 10.1016/j.cageo.2012.09.004
- 857 Hansen, T. M., Cordua, K. S., Zunino, A., & Mosegaard, K. (2016). Probabilitic
858 Integration of Geo-Information. In M. Moorekamp (Ed.), *Joint inversion*
859 (Vol. 218). John Wiley & Sons.
- 860 Hansen, T. M., & Minsley, B. J. (2019). Inversion of airborne EM data with an ex-
861 plicit choice of prior model. *Geophysical Journal International*, *218*(2), 1348–
862 1366.
- 863 Hansen, T. M., Mosegaard, K., & Cordua, K. C. (2008). Using geostatistics to
864 describe complex a priori information for inverse problems. In J. M. Ortiz &
865 X. Emery (Eds.), *Viii international geostatistics congress* (Vol. 1, p. 329–338).
866 Mining Engineering Department, University of Chile.
- 867 Hastings, W. K. (1970). Monte Carlo sampling methods using Markov chains and
868 their applications. *Biometrika*, *57*(1), 97.
- 869 Hornik, K., Stinchcombe, M., & White, H. (1990). Universal approximation of an
870 unknown mapping and its derivatives using multilayer feedforward networks.
871 *Neural networks*, *3*(5), 551–560.
- 872 Howard, D. (2020). Geological survey of western australia: Ausaem20-wa project.
873 *Preview*, *2020*(205), 18–18.
- 874 Kingma, D. P., & Ba, J. (2014). Adam: A method for stochastic optimization. *arXiv*
875 *preprint arXiv:1412.6980*.
- 876 Köpke, C., Irving, J., & Elsheikh, A. H. (2018). Accounting for model error in
877 Bayesian solutions to hydrogeophysical inverse problems using a local basis
878 approach. *Advances in Water Resources*, *116*, 195–207.
- 879 Laloy, E., Héroult, R., Jacques, D., & Linde, N. (2018). Training-image based geo-
880 statistical inversion using a spatial generative adversarial neural network. *Wa-
881 ter Resources Research*, *54*(1), 381–406.
- 882 Laloy, E., & Vrugt, J. A. (2012). High-dimensional posterior exploration of hydro-
883 logic models using multiple-try dream (zs) and high-performance computing.
884 *Water Resources Research*, *48*(1).
- 885 Madsen, R. B., & Hansen, T. M. (2018). Estimation and accounting for the mod-
886 eling error in probabilistic linearized amplitude variation with offset inversion.
887 *Geophysics*, *83*(2), N15–N30.
- 888 Malinverno, A. (2002). Parsimonious Bayesian Markov chain Monte Carlo inversion
889 in a nonlinear geophysical problem. *Geophysical Journal International*, *151*(3),
890 675–688.
- 891 Meier, U., Curtis, A., & Trampert, J. (2007). Global crustal thickness from neu-
892 ral network inversion of surface wave data. *Geophysical Journal International*,
893 *169*(2), 706–722.
- 894 Menke, W. (2012). *Geophysical data analysis: Discrete inverse theory* (Vol. 45).
895 Academic Press.
- 896 Metropolis, N., Rosenbluth, M., Rosenbluth, A., Teller, A., & Teller, E. (1953).
897 Equation of state calculations by fast computing machines. *J. Chem. Phys.*,
898 *21*, 1087–1092.
- 899 Minsley, B., Rigby, J., James, S., Burton, B., Knierim, K., Pace, M., . . . Kress, W.
900 (2021). *Closing a scale-gap in earth observation using regional-scale airborne*
901 *geophysics in the lower mississippi valley* (Tech. Rep.). Copernicus Meetings.
- 902 Minsley, B. J. (2011). A trans-dimensional Bayesian Markov chain Monte Carlo
903 algorithm for model assessment using frequency-domain electromagnetic data.
904 *Geophysical Journal International*, *187*(1), 252–272.

- 905 Minsley, B. J., Foks, N. L., & Bedrosian, P. A. (2021). Quantifying model structural
 906 uncertainty using airborne electromagnetic data. *Geophysical Journal Interna-*
 907 *tional*, *224*(1), 590–607.
- 908 Minsley, B. J., Rigby, J. R., James, S. R., Burton, B. L., Knierim, K. J., Pace,
 909 M. D., . . . Kress, W. H. (2021). Airborne geophysical surveys of the lower
 910 mississippi valley demonstrate system-scale mapping of subsurface architecture.
 911 *Communications Earth & Environment*, *2*(1), 1–14.
- 912 Moghadas, D. (2020). One-dimensional deep learning inversion of electromagnetic in-
 913 duction data using convolutional neural network. *Geophysical Journal Interna-*
 914 *tional*, *222*(1), 247–259.
- 915 Moghadas, D., Behroozmand, A. A., & Christiansen, A. V. (2020). Soil electrical
 916 conductivity imaging using a neural network-based forward solver: Applied to
 917 large-scale bayesian electromagnetic inversion. *Journal of Applied Geophysics*,
 918 104012.
- 919 Mosegaard, K., & Tarantola, A. (1995). Monte Carlo sampling of solutions to inverse
 920 problems. *J. geophys. Res.*, *100*(B7), 12431–12447.
- 921 Mosser, L., Dubrule, O., & Blunt, M. J. (2017). Reconstruction of three-dimensional
 922 porous media using generative adversarial neural networks. *Physical Review E*,
 923 *96*(4), 043309.
- 924 Mosser, L., Dubrule, O., & Blunt, M. J. (2020). Stochastic seismic waveform inver-
 925 sion using generative adversarial networks as a geological prior. *Mathematical*
 926 *Geosciences*, *52*(1), 53–79.
- 927 Puzyrev, V., & Swidinsky, A. (2019). Inversion of 1d frequency-and time-domain
 928 electromagnetic data with convolutional neural networks. *arXiv preprint*
 929 *arXiv:1912.00612*.
- 930 Rimstad, K., Avseth, P., & Omre, H. (2012). Hierarchical Bayesian lithology/fluid
 931 prediction: A North Sea case study. *Geophysics*, *77*(2), B69–B85.
- 932 Röth, G., & Tarantola, A. (1994). Neural networks and inversion of seismic data.
 933 *Journal of Geophysical Research: Solid Earth*, *99*(B4), 6753–6768.
- 934 Sambridge, M., Bodin, T., Gallagher, K., & Tkalčić, H. (2013). Transdimensional
 935 inference in the geosciences. *Philosophical Transactions of the Royal Society A:*
 936 *Mathematical, Physical and Engineering Sciences*, *371*(1984), 20110547.
- 937 Scales, J. A., & Snieder, R. (1997). To [b]ayes or not to [b]ayes? *Geophysics*, *62*(4),
 938 1045–1046.
- 939 Scheidt, C., Renard, P., & Caers, J. (2015). Prediction-focused subsurface modeling:
 940 investigating the need for accuracy in flow-based inverse modeling. *Mathemati-*
 941 *cal Geosciences*, *47*(2), 173–191.
- 942 Shahraeeni, M. S., & Curtis, A. (2011). Fast probabilistic nonlinear petrophysical in-
 943 version. *Geophysics*, *76*(2), E45–E58.
- 944 Smith, B. D., Abraham, J. D., Cannia, J. C., Minsley, B. J., Deszcz-Pan, M., & Ball,
 945 L. B. (2010). *Helicopter electromagnetic and magnetic geophysical survey*
 946 *data, portions of the North Platte and South Platte Natural Resources Dis-*
 947 *tricts, Western Nebraska* (Tech. Rep. No. 2010-1259). U.S. Geological Survey
 948 Scientific Investigations Report. doi: 10.3133/ofr20101259
- 949 Tarantola, A. (2005). *Inverse problem theory and methods for model parameter esti-*
 950 *mation*. SIAM.
- 951 Tarantola, A., & Valette, B. (1982a). Generalized nonlinear inverse problems solved
 952 using the least squares criterion. *Rev. Geophys. Space Phys.*, *20*(2), 219–232.
- 953 Tarantola, A., & Valette, B. (1982b). Inverse problems= quest for information. *J.*
 954 *Geophys.*, *50*(3), 150–170.
- 955 Tikhonov, A. N. (1963). On the solution of ill-posed problems and the method of
 956 regularization. In *Doklady akademii nauk* (Vol. 151, pp. 501–504).
- 957 Viezzoli, A., Christiansen, A. V., Auken, E., & Sørensen, K. (2008). Quasi-3D mod-
 958 eling of airborne TEM data by spatially constrained inversion. *Geophysics*,
 959 *73*(3), F105–F113.

- 960 Vilhelmsen, T. N., Auken, E., Christiansen, A. V., Barfod, A. S., Marker, P. A.,
961 & Bauer-Gottwein, P. (2019). Combining clustering methods with mps to
962 estimate structural uncertainty for hydrological models. *Frontiers in Earth*
963 *Science*, *7*, 181.
- 964 Zhang, X., & Curtis, A. (2020a). Seismic tomography using variational in-
965 ference methods. *Journal of Geophysical Research: Solid Earth*, *125*(4),
966 e2019JB018589.
- 967 Zhang, X., & Curtis, A. (2020b). Variational full-waveform inversion. *Geophysical*
968 *Journal International*, *222*(1), 406–411.
- 969 Zhang, X., & Curtis, A. (2021). Bayesian geophysical inversion using invertible
970 neural networks. *Journal of Geophysical Research: Solid Earth*, *126*(7),
971 e2021JB022320.
- 972 Zhao, X., Curtis, A., & Zhang, X. (2022). Bayesian seismic tomography using nor-
973 malizing flows. *Geophysical Journal International*, *228*(1), 213–239.